Article

TRANSPARENT PROCESS OPEN ACCESS

EMBO reports

CHK1-CDC25A-CDK1 regulate cell cycle progression and protect genome integrity in early mouse embryos

Lucie Knoblochova[1,2], Tomas Duricek[1], Michaela Vaskovicova[1], Chrysoula Zorzompokou[1], Diana Rayova[1], Ivana Ferencova[1], Vladimir Baran[3], Richard M Schultz[4,5], Eva R Hoffmann[6] & David Drutovic[1,*]

Abstract

After fertilization, remodeling of the oocyte and sperm genomes is essential to convert these highly differentiated and transcriptionally quiescent cells into early cleavage-stage blastomeres that are transcriptionally active and totipotent. This developmental transition is accompanied by cell cycle adaptation, such as lengthening or shortening of the gap phases G1 and G2. However, regulation of these cell cycle changes is poorly understood, especially in mammals. Checkpoint kinase 1 (CHK1) is a protein kinase that regulates cell cycle progression in somatic cells. Here, we show that CHK1 regulates cell cycle progression in early mouse embryos by restraining CDK1 kinase activity due to CDC25A phosphatase degradation. CHK1 kinase also ensures the long G2 phase needed for genome activation and reprogramming gene expression in two-cell stage mouse embryos. Finally, *Chk1* depletion leads to DNA damage and chromosome segregation errors that result in aneuploidy and infertility.

Keywords CDC25A phosphatase; CDK1 kinase; cell cycle regulation; CHK1 kinase; early mouse embryos

Subject Categories Cell Cycle; Chromatin, Transcription & Genomics; Development

DOI 10.15252/embr.202256530 | Received 23 November 2022 | Revised 17 August 2023 | Accepted 18 August 2023 | Published online 11 September 2023

EMBO Reports (2023) 24: e56530

Introduction

Preimplantation development is associated with several critical developmental changes that include initial embryonic cell divisions, zygotic genome activation, compaction, and blastocyst formation. The egg and sperm are highly differentiated cells whose chromatin structure has dramatically different epigenetic landscapes (Kobayashi *et al*, 2012; Eckersley-Maslin *et al*, 2018; Sankar *et al*, 2020). Following fertilization, these differences are resolved largely during the first cell cycle as the paternal and maternal genomes are remodeled to provide a chromatin structure that supports the dramatic reprogramming of gene expression associated with genome activation (Eckersley-Maslin *et al*, 2018). These processes are linked to significant cell cycle changes and regulated by maternally derived proteins and mRNAs stored in the egg until transcription from the embryonic genome is established.

The first two embryonic cell divisions are about 18–20 h long in mouse and human embryos. Duration of individual cell cycle phases in initial embryonic cell divisions differs mainly in the length of the gap phases. In contrast to the zygotic G1 phase, which lasts about 5–12 h, dependent on the genetic background, two-cell stage embryos spend only 1–2 h in G1. Lengthening the first G1 phase likely provides sufficient time to form both pronuclei, which requires chromatin decondensation of the egg and sperm nuclei and chromatin remodeling (Artus & Cohen-Tannoudji, 2008; Palmer & Kaldis, 2016; Radonova *et al*, 2019). In mice, transcription of the embryonic genome starts during the first S phase in the zygote and slowly increases from G2 ("minor" genome activation) to a peak in G2 in late two-cell stage embryos ("major" genome activation; Braude, 1979; Flach *et al*, 1982; Molls *et al*, 1983; Aoki *et al*, 1997). The second cell cycle is characterized by a very short G1 phase (approximately 1–2 h) and a dramatic lengthening of G2/M transition (approximately 12–16 h) compared to 1–8 h for G2/M in the first cell cycle (Abramczuk & Sawicki, 1975; Krishna & Generoso, 1977; Domon, 1980; Molls *et al*, 1983; Howlett & Bolton, 1985; Palmerola *et al*, 2022). This extended G2 phase likely provides sufficient time for expression of products of major genome

1 Institute of Animal Physiology and Genetics of the Czech Academy of Sciences, Libechov, Czech Republic
2 Faculty of Science, Charles University, Prague, Czech Republic
3 Institute of Animal Physiology, Centre of Biosciences, Slovak Academy of Sciences, Kosice, Slovakia
4 Department of Biology, University of Pennsylvania, Philadelphia, PA, USA
5 Department of Anatomy, Physiology, and Cell Biology, School of Veterinary Medicine, University of California, Davis, CA, USA
6 DNRF Center for Chromosome Stability, Department of Cellular and Molecular Medicine, Faculty of Health and Medical Sciences, University of Copenhagen, Copenhagen, Denmark
*Corresponding author. Tel: +420 315 639 561; E-mail: drutovic@iapg.cas.cz

activation to accumulate to sufficient concentrations and thereby supports continued development (Flach *et al*, 1982; Molls *et al*, 1983). Genome activation in other mammals occurs at the 4- to 16-cell stage, although there is evidence for earlier transcription (Xue *et al*, 2013; Graf *et al*, 2014; Li *et al*, 2020). Mechanisms underlying regulation of cell cycle duration in the initial divisions of early mammalian development, in particular the transition from a long G1 and short G2 in zygotes to a short G1 and long G2 in two-cell embryos, remain largely unknown.

Cell cycle progression is largely regulated by cyclin-dependent kinases (CDK). CDKs are inhibited by WEE/MYT kinase-mediated phosphorylation of T14 or Y15. To activate CDKs, these inhibitory phosphorylations are removed by CDC25 phosphatases (Enoch & Nurse, 1990). Although CDKs in mammals have many paralogues—*Cdk1*, *Cdk2*, *Cdk4*, *Cdk6*, and others—, CDK1 is the only essential one (Santamaría *et al*, 2007). CDK1 can compensate for the other CDKs and is indispensable for meiotic (Adhikari *et al*, 2012) and mitotic progression (Santamaría *et al*, 2007). *Cdc25* phosphatase in mammals has three paralogues, *Cdc25a*, *Cdc25b*, and *Cdc25c* (Sadhu *et al*, 1990; Galaktionov & Beach, 1991; Nagata *et al*, 1991), with CDC25A being the only essential one (Chen *et al*, 2001; Lincoln *et al*, 2002; Ferguson *et al*, 2005; Ray *et al*, 2007; Lee *et al*, 2009).

Genome integrity relies on communication between the cell cycle progression, checkpoint activation, and DNA repair pathways. DNA damage activates the DNA damage response (DDR) and cell cycle checkpoint signaling, which retards cell cycle progression to ensure sufficient time to repair DNA damage. Interestingly, the ability of cell cycle checkpoint signaling proteins to modulate cell cycle duration is utilized for early development (Artus & Cohen-Tannoudji, 2008). However, little is known about DDR signaling and checkpoint activation in early embryos. It should be noted that incompletely replicated DNA caused by replication stress during human embryonic development is a major cause of an increased incidence of aneuploidy in human embryos (Palmerola *et al*, 2022).

ATR and CHK1 are DDR kinases that regulate cell cycle progression by maintaining replication checkpoint signaling (Kalogeropoulos *et al*, 2004; Zachos *et al*, 2005; Eykelenboom *et al*, 2013; Saldivar *et al*, 2018; Lebrec *et al*, 2022). The replication checkpoint prevents mitosis before DNA replication is finished (Hartwell & Weinert, 1989; Enoch & Nurse, 1990). CHK1, not ATR, is the DDR-limiting kinase in the zygote (Ladstätter & Tachibana-Konwalski, 2016). In addition, CHK1 depletion or inhibition results in premature mitosis and chromosome fragmentation in mice (Lam *et al*, 2004; Niida *et al*, 2005; Peddibhotla *et al*, 2009; Fishler *et al*, 2010), avian (Zachos *et al*, 2003, 2005, 2007), and human (Niida *et al*, 2005; Syljuåsen *et al*, 2005; Durkin *et al*, 2006; Branigan *et al*, 2021) somatic cells. CHK1 also regulates cell cycle progression during embryonic development in zebrafish (Dalle Nogare *et al*, 2009; Zhang *et al*, 2014), *Drosophila* (Deneke *et al*, 2016), and *Xenopus* (Shimuta *et al*, 2002; Petrus *et al*, 2004). Moreover, CHK1 inhibition or depletion in human (Palmerola *et al*, 2022) and mouse embryos (Liu *et al*, 2000; Takai *et al*, 2000; Ju *et al*, 2020) exacerbates the incidence of aneuploidy and induces genome fragmentation.

Although the mechanism underlying the role of CHK1 in cell cycle checkpoint signaling is well understood in somatic cells, little is known regarding the function of CHK1 signaling in regulating embryonic cell division and genome integrity in early mammalian embryos. Here, we show that maternal *Chk1* depletion in mice causes acceleration of cell cycle progression accompanied by severe chromosome segregation errors, especially in two-cell embryos. Live-cell imaging revealed that maternal *Chk1* depletion shortens all cell cycle phases in two-cell embryos, most notably, the long G2 phase needed for genome activation. The shortening is due to premature CDK1 kinase activation caused by stabilization of CDC25A phosphatase.

Results

Maternally expressed *Chk1* regulates duration of the first and second cleavage divisions

We previously reported that maternally expressed *Chk1* is not required for oocyte maturation but is essential for preimplantation development in mice (Ruth *et al*, 2021); maternally depleted *Chk1* embryos show impaired development to the blastocyst stage, massive genome fragmentation at the three- to four- or five- to eight-cell stage, and a lack of liveborn pups. To further understand the maternal contribution of CHK1 during preimplantation development, we used the same mouse model where Cre recombinase is expressed using the zona pellucida-3 (*Zp3*) promoter to remove floxed exon 2 of *Chk1* in growing oocytes (Lam *et al*, 2004; Ruth *et al*, 2021; Fig EV1A and B). Females lacking *Chk1* in oocytes were mated with wild-type (WT) males to produce maternally depleted *Chk1* embryos (*Chk1* mKO; Fig EV1C). Controls were litter mates carrying a floxed exon 2 but not Cre recombinase, which results in CHK1 expression as in WT (*Chk1* WT; Fig EV1C). Immunoblot analysis showed that CHK1 protein was not detected in WT sperm (Fig EV1D), thereby minimizing any paternal contribution to *Chk1* mKO embryos. We observed low expression of full-length and truncated CHK1 in *Chk1* mKO zygotes (Fig EV1E). The truncated CHK1 version may have arisen by initiating translation from the first methionine reside encoded in exon 3, which would yield CHK1 lacking the initial 41 amino acids (*Chk1* Δ^2) and giving rise to a species with a predicted band size of 50 kDa, which was observed on the immunoblot (Fig EV1B and E).

To analyze the role of CHK1 in cell cycle progression during preimplantation development, bright-field images of live, *Chk1* WT, and *Chk1* mKO embryos were collected every 30 min, and individual embryos were analyzed for cell cycle progression (Fig 1A and B; Nothias *et al*, 1995; Artus & Cohen-Tannoudji, 2008). At 114 h after hCG administration, 53% of *Chk1* WT zygotes formed blastocysts, compared to 12% of *Chk1* mKO zygotes (Fig 1C). In addition, *Chk1* mKO embryos exhibited an increase in cellular fragmentation (Fig 1B and C). Blastocysts that formed from *Chk1* mKO embryos could develop further because some dead pups, but no live pups, were born (Ruth *et al*, 2021). We confirmed these results by culturing zygotes in the presence of 250 nM CHIR-124, a CHK1 inhibitor (Tse *et al*, 2007), and observed embryonic arrest and failure to form blastocysts (Fig EV1F). This phenotype was observed both in C57J/BL6 and CD-1 mouse strain backgrounds (Fig EV1F).

Bright-field time-lapse data revealed that *Chk1* mKO zygotes divided to the two-cell stage about 2 h earlier than *Chk1* WT, and these mutant embryos also divided sooner (measured as two-cell to three-cell stage division; Fig 1D and E), with 54% dividing 13 h earlier than *Chk1* WT (hereafter referred to as *Chk1* mKO *class I*; Fig 1C

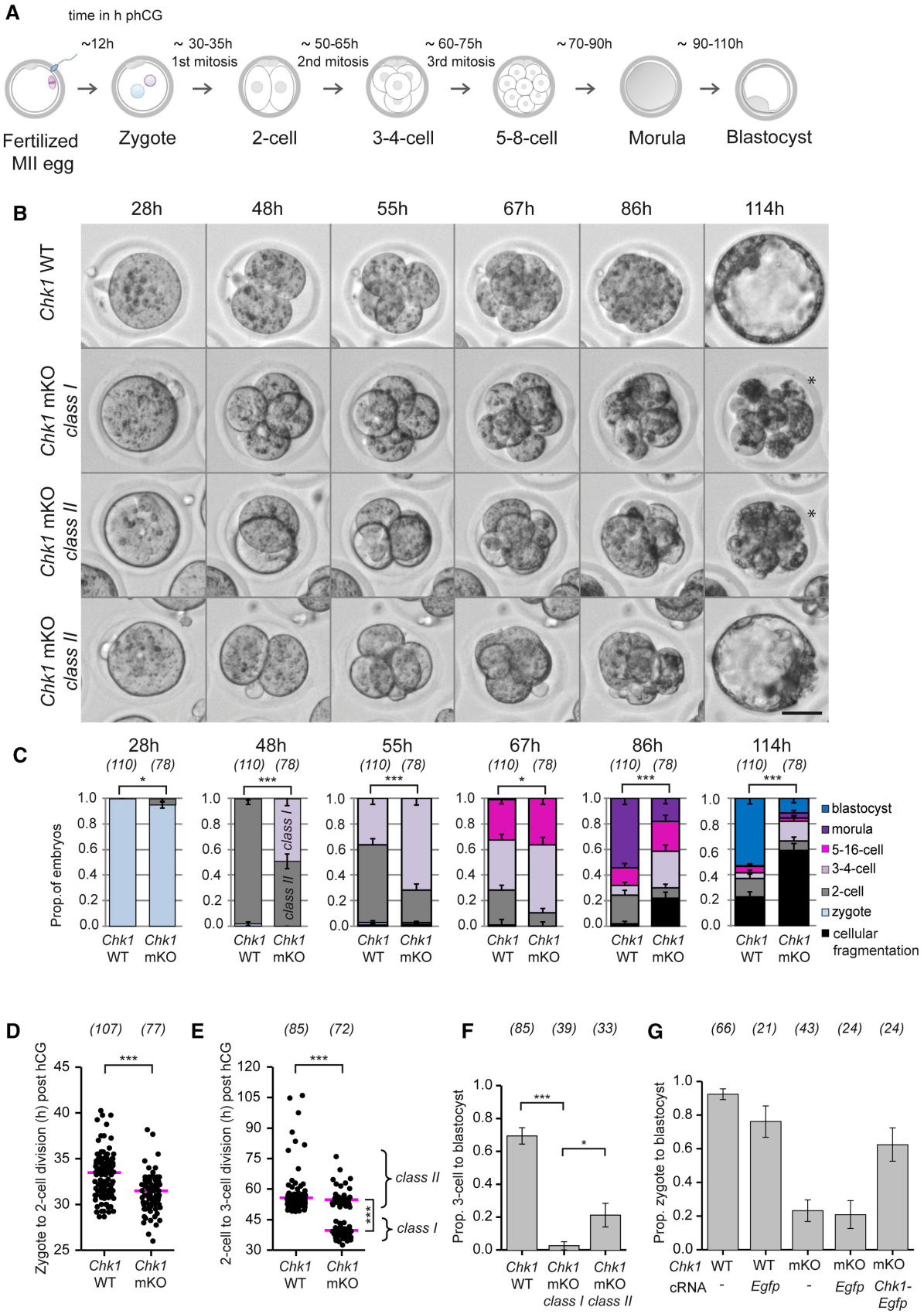
A
time in h phCG
~12h
~ 30-35h
1st mitosis
~ 50-65h
2nd mitosis
~ 60-75h
3rd mitosis
~ 70-90h
~ 90-110h
Fertilized MII egg
Zygote
2-cell
3-4-cell
5-8-cell
Morula
Blastocyst
B
28h
48h
55h
67h
86h
114h
Chk1 WT
Chk1 mKO class I
Chk1 mKO class II
Chk1 mKO class II
C
28h
48h
55h
67h
86h
114h
(110) (78)
Prop.of embryos
Chk1 WT
Chk1 mKO
class I
class II
blastocyst
morula
5-16-cell
3-4-cell
2-cell
zygote
cellular fragmentation
D
(107) (77)
Zygote to 2-cell division (h) post hCG
E
(85) (72)
2-cell to 3-cell division (h) post hCG
class II
class I
F
(85) (39) (33)
Prop. 3-cell to blastocyst
class I class II
G
(66) (21) (43) (24) (24)
Prop. zygote to blastocyst
Chk1 cRNA
WT -
WT Egfp
mKO -
mKO Egfp
mKO Chk1-Egfp

Figure 1.

Figure 1. *Chk1* mKO embryos display accelerated first and second embryonic division and compromised development.

A Schematic of embryonic development using bright-field time-lapse imaging. Time (h) is relative to h post-hCG administration.

B Representative still images from bright-field time-lapse imaging of preimplantation development of *Chk1* WT, *Chk1* mKO *class I*, and *Chk1* mKO *class II* embryos from 28 to 114 h post-hCG administration. Strain background: C57J/BL6, with small part CD-1. An asterisk marks fragmented embryos. Scale bar 30 μm.

C Data from bright-field time-lapse imaging (B) were used to quantify the proportion of *Chk1* WT and *Chk1* mKO embryos at different developmental stages. At 48 h, the proportion of *Chk1* mKO *class I* and *Chk1* mKO *class II* embryos is shown. Error bars denote the standard error of proportion. The numbers in parentheses show the number of embryos imaged for each genotype. The data were pooled from three independent experiments. *$P = 0.01636$ (28 h); ***$P < 0.00000$ (48 h); ***$P = 0.00005$ (55 h); *$P = 0.04435$ (67 h); ***$P = 0.00004$ (86 h); ***$P < 0.00000$ (114 h; Cochran–Armitage trend test, any trend).

D, E Data from bright-field time-lapse imaging (B) was used for quantification of the division time (h) from zygote to two-cell (D) and from two-cell to three-cell (E) in *Chk1* WT, and *Chk1* mKO, embryos. Distribution of *Chk1* mKO *class I*, and *Chk1* mKO *class II* is shown in (E). The median is shown. The data were pooled from three independent experiments. ***$P = 0.00000$ relative to the *Chk1* WT group (Mann–Whitney *U* test, two-sided), ***$P = 0.000000$ relative to the *Chk1* mKO *class I* group (Kolmogorov–Smirnov test, two-sided).

F Data from bright-field time-lapse imaging (B) was used to quantify the proportion of three-cell embryos that developed to the blastocyst stage. Error bars denote standard error of proportion. The data were pooled from three independent experiments. *$P = 0.0202$ and ***$P = 0.00000$ (Fisher's exact test).

G Proportion of *in vitro* blastocyst development in *Chk1* WT (WT) and *Chk1* mKO (mKO) zygotes microinjected with *Chk1-Egfp* or *Egfp* cRNA. Error bars denote the standard error of proportion. The data were pooled from two experiments, one with *Chk1* mKO and *Chk1-Egfp* cRNA microinjection and the other with *Chk1* mKO and *Egfp* cRNA microinjection. In both experiments, the embryos from one group were divided into microinjected and non-microinjected (serving as controls) arms.

and E). The 46% of *Chk1* mKO embryos that divided with similar timing as *Chk1* WT are referred to as *Chk1* mKO *class II* (Fig 1C and E). *Chk1* mKO *class I* showed both acceleration in the first (zygote to two-cell; Fig EV1G) and second (two- to three-cell) divisions (Fig 1E) that was accompanied by a near absence of blastocyst development (Fig 1F). Although *Chk1* mKO *class II* embryos displayed the *Chk1* WT-like timing of divisions (Figs 1E and EV1G), only about 20% developed to form blastocysts (Fig 1F). Reduced blastocyst formation was due to loss of maternal CHK1 because microinjecting *Chk1* mKO zygotes with *Chk1-Egfp* cRNA, but not *Egfp* cRNA, rescued the mutant phenotype (Fig 1G). In addition, a positive correlation was observed between the timing of the first and second embryonic division in *Chk1* mKO *class I* embryos (Fig EV1H).

To ascertain whether differences in the residual amount of CHK1 in *Chk1* mKO embryos were the basis for the *class I* or *class II* phenotype, we performed a CHK1 immunoblot analysis using embryos harvested 47–48 h post-hCG (Fig EV1I). *Chk1* mKO embryos showed a slightly higher amount of CHK1 in *Chk1* mKO *class II* embryos compared to *Chk1* mKO *class I* embryos, suggesting that the *Chk1* mKO *class II* phenotype was caused by some residual CHK1 protein compared to *Chk1* mKO *class I*. Because we did not detect expression of the truncated CHK1 version in these two classes in contrast to *Chk1* mKO zygotes (Fig EV1B and E), it was unlikely that the truncated form plays a significant role in *Chk1* mKO embryos. To further investigate the distinction between *Chk1* mKO *class I* and *class II* embryos, we assed Cre-mediated DNA recombination status using a single-cell PCR to distinguish between non-recombined and recombined *Chk1* alleles (Fig EV1J). When the substrate for the PCR is the non-recombined allele, the expected size of the amplification product is a 2.2 kb fragment, whereas when the substrate is the recombined allele, it is a 0.4 kb fragment. We show that Cre-mediated recombination of the *Chk1* gene apparently occurs in all analyzed *Chk1* mKO *class I* and *class II* embryos, where only the 0.4 kb fragment was detected in each sample (Fig EV1J). We then assessed the proportion of *Chk1* mKO *class I* embryos in individual mice. Because most mice showed 50–80% of *Chk1* mKO *class I* embryos (Fig EV1K), we conclude that full-length maternally derived CHK1 regulates the timing of initial embryonic divisions and is required for preimplantation development to blastocyst.

CHK1 kinase does not participate in completing the main phase of DNA replication

In somatic cells, CHK1 kinase prevents mitotic entry until DNA replication is completed (Kalogeropoulos *et al*, 2004; Zachos *et al*, 2005; Saldivar *et al*, 2018; Lebrec *et al*, 2022). CHK1 kinase also regulates S phase progression, including replication origin firing, replication fork speed progression, and DNA damage response in S phase (Niida *et al*, 2005; Syljuåsen *et al*, 2005; Dandoulaki *et al*, 2018; Michelena *et al*, 2019). To determine whether the accelerated zygote to two-cell division occurs prior to completion of DNA replication, we assayed DNA replication in *Chk1* mKO embryos by DAPI staining. Because CHK1 depletion increases DNA damage (Niida *et al*, 2005; Dandoulaki *et al*, 2018), we also assessed in the same embryo formation of DNA double-stranded breaks (DSBs) by immunofluorescence detection of phosphorylated histone H2AX on S139 (γH2AX; Fig EV2A; Sedelnikova *et al*, 2002; Mah *et al*, 2010). DNA replication triggers transient DDR signaling with a high γH2AX signal in S phase (Xu *et al*, 2015). Accordingly, embryos were treated with a 60 min pulse of the thymidine analog 5-ethynyl-2-deoxyuridine (EdU) to exclude zygotes in S phase from analysis (Fig EV2A) and fixed zygotes when most *Chk1* WT embryos were in G2 (Fig 1A; Artus & Cohen-Tannoudji, 2008), that is, at 28 h post-hCG administration. EdU staining also allowed us to monitor cell cycle progression.

We did not observe massive DNA underreplication in *Chk1* mKO zygotes compared to *Chk1* WT zygotes (Fig EV2B). Analysis of zygotes in G2 revealed a similar and relatively broad distribution of γH2AX foci in *Chk1* WT and *Chk1* mKO (Fig EV2C). As expected from bright-field imaging (Fig 1D), we observed a significantly different distribution of cell cycle phases in *Chk1* mKO zygotes compared to *Chk1* WT (Fig EV2D). The significant decrease in the percentage of S-phase *Chk1* mKO zygotes suggests a shortened G1 and/or S phase in zygotes lacking maternal CHK1. Taken together, *Chk1* mKO zygotes show neither massive DNA underreplication nor elevated DSBs but do exhibit altered cell cycle progression and accelerated G2/M entry.

To gain insight into the basis for the accelerated second division in *Chk1* mKO embryos, we examined DNA content, DSBs formation, and cell cycle progression in late two-cell stage embryos. We fixed

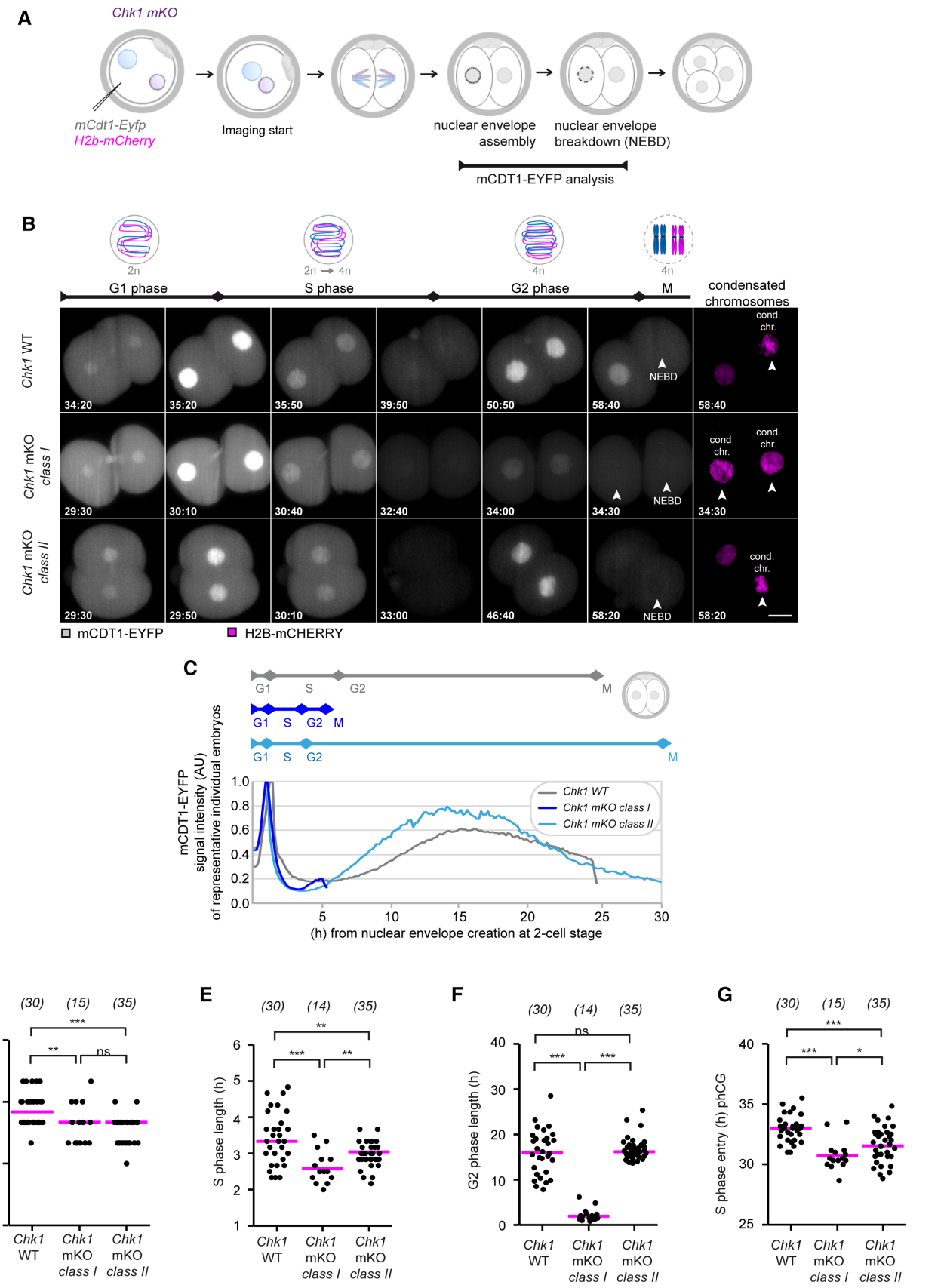
A
Chk1 mKO
mCdt1-Eyfp
H2b-mCherry
Imaging start
nuclear envelope assembly
nuclear envelope breakdown (NEBD)
mCDT1-EYFP analysis
B
2n
2n → 4n
4n
4n
G1 phase
S phase
G2 phase
M
condensated chromosomes
Chk1 WT
Chk1 mKO class I
Chk1 mKO class II
cond. chr.
NEBD
34:20
35:20
35:50
39:50
50:50
58:40
29:30
30:10
30:40
32:40
34:00
34:30
29:50
33:00
46:40
58:20
mCDT1-EYFP
H2B-mCHERRY
C
G1 S G2 M
mCDT1-EYFP signal intensity (AU) of representative individual embryos
Chk1 WT
Chk1 mKO class I
Chk1 mKO class II
(h) from nuclear envelope creation at 2-cell stage
D
G1 phase length (h)
E
S phase length (h)
F
G2 phase length (h)
G
S phase entry (h) phCG
(30)
(15)
(14)
(35)
ns
Chk1 WT
Chk1 mKO class I
Chk1 mKO class II

Figure 2.

Figure 2. CHK1 kinase regulates cell cycle progression in G1, S, G2, and mitosis.

A Schematic representation of the experimental design.

B Representative still images from time-lapse light-sheet imaging of preimplantation development of *Chk1* WT, *Chk1* mKO *class I*, and *Chk1* mKO *class II* embryos. Embryos were microinjected, as shown in (A). Embryos expressing mCDT1-EYFP (gray) and H2B-mCHERRY (magenta, chromosomes) are shown. Time points are relative to time post-hCG administration (h). Arrowheads show condensated chromosomes after NEBD. Scale bar 20 μm. See also related Movie EV2 (*Chk1* WT + *mCdt1-Egfp*, *Chk1* mKO *class I* + *mCdt1-Egfp*, and *Chk1* mKO *class II* + *mCdt1-Egfp*).

C Representative line charts of fluorescence signal intensity of mCDT1-EYFP sensor in individual two-cell stage embryos from time-lapse light-sheet imaging (as shown in B) from nuclear envelope formation to nuclear envelope breakdown. Above is a schematic depiction of the cell cycle phase length derived from the line chart.

D–G Data from time-lapse light-sheet imaging (B) was used to quantify the length (h) of G1 (D), S (E), and G2 phase (F), and S phase beginning (h from hCG stimulation) (G) of two-cell stage embryos. The data were pooled from three independent experiments. The numbers in parentheses show the number of embryos per group. The median is shown. Statistics are as follows: (D) $^{**}P = 0.00803$ (equal-variance *T*-test), $^{***}P = 0.00000$, and ns, non-significant $P = 0.52152$ (Aspin–Welch unequal-variance *T*-test). (E) $^{***}P = 0.00068$ and $^{**}P = 0.00718$ for *Chk1 mKO class I* (equal-variance *T*-test). $^{**}P = 0.00354$ for *Chk1 WT* (Aspin-Welch unequal-variance *T*-test). (F) $^{***}P = 0.00000$, and ns, non-significant $P = 0.087335$ (Kolmogorov–Smirnov test). (G) $^{***}P = 0.0000$ (*Chk1* WT vs. *Chk1* mKO *class I*), $^{***}P = 0.00018$ (*Chk1* WT vs. *Chk1* mKO *class II*), and $^{*}P = 0.04969$ (equal-variance *T*-test).

the embryos at 50 h after hCG administration when *Chk1* WT and *Chk1* mKO *class II* embryos should be in the two-cell stage, but *Chk1* mKO *class I* should be in the three- or four-cell stage (Fig 1B and C). Consistent with our previous results, *Chk1* mKO showed *class I* (three- to four-cell stage) and *class II* (two-cell stage embryos; Fig EV2E and F) distributions, with *Chk1* mKO *class I* embryos showing significant increase in genome fragmentation and micronuclei formation (Fig EV2E and G). A 60-min EdU pulse revealed that all two-cell embryos were in G2 (Fig EV2E). In addition, DNA content (assayed by DAPI staining) in two-cell stage *Chk1* mKO *class II* embryos was similar to two-cell stage *Chk1* WT (Fig EV2H), whereas DSBs formation (assayed by γH2AX detection) was greater than *Chk1* WT (Fig EV2I). Thus, *Chk1* mKO *class II* embryos do not show massive DNA underreplication but exhibit increased DNA damage. Our results suggest that CHK1 does not participate in completing the main phase of DNA replication and entry into G2 and subsequent mitosis in early cleavage-stage mouse embryos because DNA content in *Chk1* mKO was similar to *Chk1* WT (Fig EV2B and H).

Apart from CHK1, WEE/MYT protein kinases also participate in replication checkpoints in somatic cells (Enoch & Nurse, 1990). To ascertain whether WEE/MYT are involved in completing DNA replication in early embryos, we used embryos from transgenic *H2b-Egfp* mice to label chromosomes for live imaging (Hadjantonakis & Papaioannou, 2004; Mayer *et al*, 2016) and treated them with the WEE/MYT kinase inhibitor PD0166285 21 h after hCG administration (Appendix Fig S1A) when the embryos were in late G1 or early S phase (Artus & Cohen-Tannoudji, 2008) and then monitored their development by light-sheet microscopy. The treated zygotes entered mitosis, detected by chromosome condensation, as early as 24 h post-hCG, when DMSO-treated embryos were in S phase (Appendix Fig S1B and C; Movie EV1). Only 8% of PD0166285-treated embryos completed mitosis and divided to the two-cell stage (Appendix Fig S1D). These results show that WEE/MYT kinases regulate mitosis entry from the early or middle S phase, in contrast to CHK1, which does not participate in completing the main phase of DNA replication in early embryos.

CHK1 kinase is required for the long G2 phase in two-cell stage embryos

We next examined in more detail the accelerated cell cycle progression in two-cell *Chk1* mKO embryos. We microinjected *Chk1* WT and *Chk1* mKO zygotes with cRNAs for histone *H2b-mCherry* to monitor chromosomes and a modified Fucci (CA) sensor (*mCdt1-Eyfp*) to monitor cell cycle progression (Fig 2A). Because mCDT1-EYFP is degraded during S phase, reappears in G2, and disperses in the cytoplasm after nuclear envelope breakdown (NEBD), we could distinguish the duration of each cell cycle phase in *Chk1* WT and *Chk1* mKO two-cell embryos (Fig 2B and C; Movie EV2).

To validate the information about cell cycle progression from the mCDT1-EYFP sensor, we compared these data to cell cycle progression measured by EdU incorporation. Similar results were obtained with both methods, with S phase ending about 39–41 h post-hCG administration in WT embryos (Appendix Fig S1E–G). The mCDT1-EYFP signal analysis showed that both *Chk1* mKO *class I* and *class II* embryos displayed a slightly but significantly shorter G1 phase due to earlier initiation of S phase compared to *Chk1* WT (Fig 2D). Also, both *Chk1* mKO *class I* and *class II* embryos displayed a significantly shorter S phase, with *Chk1* mKO *class I* embryos having a shorter S phase than *Chk1* mKO *class II* embryos (Fig 2E). In addition, the majority of *Chk1* mKO *class I* embryos did not enter premature mitosis from S phase but from G2 (14 of 15 embryos). Duration of G2 in *Chk1* mKO *class I* embryos was also significantly shortened by about 14 h in comparison to *Chk1* mKO *class II* embryos, which showed the same G2 duration as *Chk1* WT embryos (Fig 2F). In the timing post-hCG stimulation, *Chk1* WT embryos entered S phase from 31 h to 36 h, whereas *Chk1* mKO embryos entered S phase from 29 to 35 h (Fig 2G). Altogether, these results suggest that CHK1 regulates cell cycle progression of all cell cycle phases, but most significantly, CHK1 is essential for maintaining the long G2 phase in two-cell embryos.

CHK1 kinase regulates long G2 in two-cell stage embryos by restraining CDK1 activity via CDC25A degradation

In some somatic cell lines, *Chk1* deficiency causes premature entry into mitosis due to precocious CDK1-cyclin B activation (Niida *et al*, 2005; Lemmens *et al*, 2018; Branigan *et al*, 2021). Because the naturally occurring long G2 phase in two-cell mouse embryos was shortened in *Chk1* mKO (Fig 2C and F), we asked whether the shortened G2 in *Chk1* mKO embryos was caused by premature activation of CDK1. Accordingly, we sought to see if partial CDK1 inhibition could rescue the *Chk1* mKO *class I* phenotype by allowing two-cell embryos to progress to M phase with similar timing to *Chk1* WT. This approach, namely partially inhibiting CDK1, was successfully

used to inhibit resumption of meiosis, which requires CDK1 activation (Solc *et al*, 2015; Fig EV3A). To determine whether partial CDK1 inhibition was also feasible in mouse embryos, we used different concentrations of RO-3306 (Vassilev *et al*, 2006; Spencer *et al*, 2013; Jang *et al*, 2014). Based on these results, we cultured two-cell embryos in 2.5 μM RO-3306 and followed cell cycle progression by bright-field microscopy. Treatment with 2.5 μM RO-3306, but not DMSO alone, rescued the onset of mitosis in *Chk1* mKO embryos (Fig 3A and EV3B). These findings, which show that partial inhibition of CDK1 rescues M phase timing in two-cell stage *Chk1* mKO embryos, suggest that CHK1 restrains CDK1 activity to regulate cell cycle progression.

In mammals, CDK1 is activated by cyclins and CDC25 phosphatases. CHK1 disrupts the action of all CDC25 phosphatases through

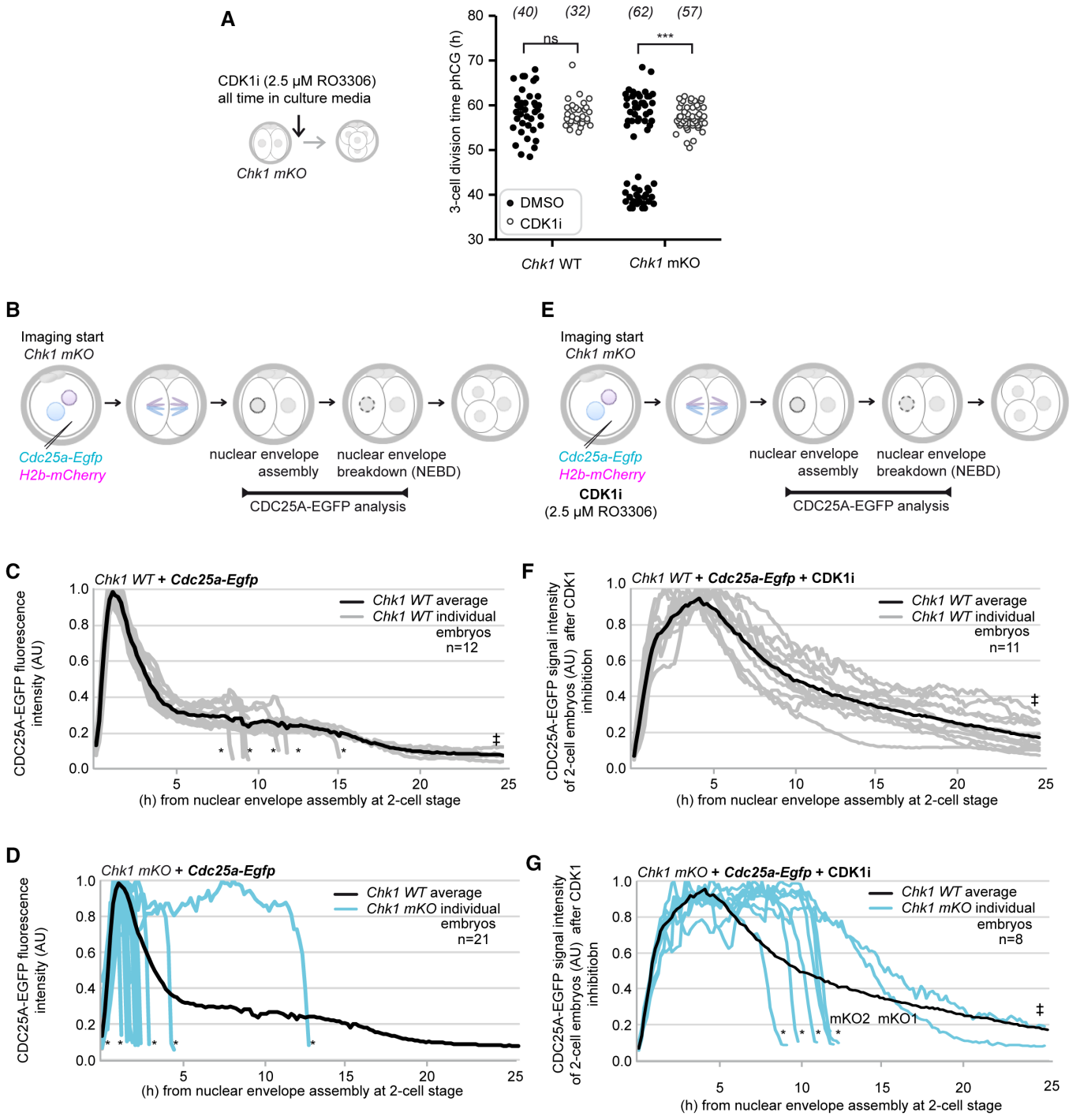

Figure 3.

Figure 3. CHK1 kinase regulates long G2 in mouse two-cell stage embryos by restraining CDK1 activity via CDC25A degradation.

A Division time (h) from two-cell to three-cell stage embryos. *Chk1* WT and *Chk1* mKO embryos were treated within 3 h after two-cell division with 2.5 μM RO3306 (CDK1 kinase inhibitor) or DMSO and imaged by bright-field time-lapse microscopy. The numbers in parentheses denote the number of embryos analyzed per group. Strain background: CD-1 with small part C57J/BL6 and C57J/BL6 with small part CD-1. The data were pooled from two independent experiments. ns, non-significant, $P = 0.145858$, and $^{***}P = 0.000031$ (Kolmogorov–Smirnov test).

B Schematics of experimental design.

C, D Line chart of fluorescence signal intensity of CDC25A-EGFP of individual *Chk1* WT (C) and *Chk1* mKO (D) two-cell stage embryos scanned using light-sheet time-lapse microscopy from nuclear envelope assembly to nuclear envelope breakdown. Embryos were microinjected as shown in (B). Asterisk marks signal drop after nuclear envelope breakdown (not degradation). ‡Points to CDC25A-EGFP signal in *Chk1* WT embryos that did not enter mitosis within 25 h after nuclear envelope assembly. The data are from one experiment with two *Chk1* WT and four *Chk1* mKO mice treated individually. The line of the *Chk1* WT average is shown. The two- to three-cell anaphase timing is shown in Fig EV3F.

E Schematics of experimental design.

F, G Line chart of fluorescence signal intensity of CDC25A-EGFP of individual *Chk1* WT (F) and *Chk1* mKO (G) two-cell stage embryos scanned using time-lapse light-sheet microscopy from nuclear envelope assembly to nuclear envelope breakdown. Embryos were microinjected and treated with 2.5 μM RO3306 (CDK1 kinase inhibitor) as shown in (E). Asterisk marks signal drop after nuclear envelope breakdown (not degradation). ‡Points to CDC25A-EGFP signal in *Chk1* WT embryos that did not enter mitosis within 25 h after nuclear envelope assembly. The data are from one experiment with four *Chk1* WT and four *Chk1* mKO mice treated in two or four groups, respectively. The line of the *Chk1* WT average is shown. The two- to three-cell anaphase timing is shown in Fig EV3H.

inhibitory phosphorylation, as in the case of CDC25B and CDC25C (Peng *et al*, 1997; Sanchez *et al*, 1997; Mailand *et al*, 2000; Chen *et al*, 2003; Sorensen *et al*, 2003; Kramer *et al*, 2004; Löffler *et al*, 2006; Schmitt *et al*, 2006; Goto *et al*, 2019), but most importantly, through degradation, as in the case of CDC25A (Mailand *et al*, 2000; Zhao *et al*, 2002; Sorensen *et al*, 2003; Goto *et al*, 2019). CHK1 depletion/inhibition causes stable CDC25A levels (Sorensen *et al*, 2003; Lam *et al*, 2004; Tse *et al*, 2007; Goto *et al*, 2019) and premature mitotic entry (Molinari *et al*, 2000; Mailand *et al*, 2002). These observations suggest that CDC25A is the major CDC25 phosphatase during early embryo development, and its stabilization after *Chk1* depletion could explain the precocious CDK1 activation and subsequent premature mitotic entry in *Chk1* mKO embryos.

To ascertain if a high CDC25A level causes premature mitotic entry, we overexpressed CDC25A by microinjecting *Cdc25a-Egfp* and *H2b-mCherry* cRNAs into WT embryos and observed premature mitosis in both the first and the second embryonic division (Fig EV3C and D). We then determined whether a high CDC25A level causes premature mitotic entry in two-cell *Chk1* mKO embryos using a similar microinjection approach and observed an accelerated first and second mitosis in both *Chk1* WT and *Chk1* mKO embryos, which was more pronounced in *Chk1* mKO embryos (Fig EV3E and F). We also monitored CDC25A-EGFP intensity from nuclear envelope assembly in the two-cell embryos until NEBD before the subsequent mitosis (Fig 3B). *Chk1* WT showed a peak in CDC25A-EGFP intensity at 1–1.5 h after nuclear envelope assembly in two-cell embryos, with a subsequent signal decline until NEBD at 8.5 h or later (Fig 3C). The timing of CDC25A-EGFP degradation was consistent with CDC25A phosphatase being degraded in S phase of two-cell embryos. *Chk1* mKO embryos microinjected with *Cdc25a-Egfp* cRNA showed an increase in CDC25A-EGFP signal intensity followed by a rapid signal decline caused by CDC25A-EGFP signal dispersion into the cytoplasm during NEBD after mitotic entry (86%, $n = 18$; Fig 3D and Appendix Fig S2A and B). These results suggest that a high CDC25A concentration causes premature mitotic entry in two-cell *Chk1* mKO embryos.

Because most *Cdc25a-Egfp* cRNA injected *Chk1* mKO embryos divided too early to analyze the CDC25A-EGFP signal before NEBD, we delayed mitotic entry by partially inhibiting CDK1 with 2.5 μM RO3306. The zygotes were microinjected with cRNAs for *Cdc25a-Egfp* and *histone H2b-mCherry* and then treated with RO3306 (Fig 3E). This protocol successfully delayed the first and the second mitosis in *Chk1* WT and *Chk1* mKO embryos (Fig EV3G and H) compared to untreated *Chk1* WT and *Chk1* mKO embryos (Fig EV3E and F). Next, we analyzed the CDC25A-EGFP signal in CDK1-inhibited two-cell embryos. CDC25A-EGFP levels decreased more slowly in CDK1-inhibited *Chk1* WT embryos (Fig 3F; Movie EV3) compared to non-inhibited *Chk1* WT embryos (Fig 3C). On the other hand, all CDK1-inhibited *Chk1* mKO embryos showed CDC25A-EGFP signal stabilization (Fig 3G) compared to non-inhibited *Chk1* mKO embryos (Fig 3D). We also noted that a subset of CDK1-inhibited *Chk1* mKO embryos (referred to as mKO1) showed WT-like timing of mitotic entry and slow decrease in CDC25A-EGFP levels similar to CDK1-inhibited *Chk1* WT embryos (Figs 3G and EV3I and J, Movie EV3). On the other hand, a subset of CDK1-inhibited *Chk1* mKO embryos (referred to as mKO2) showed accelerated NEBD followed by CDC25A-EGFP dispersion into the cytoplasm (Figs 3G and EV3I and J; Movie EV3). These results imply that CHK1 regulates mitotic entry in two-cell stage embryos by controlling CDC25A degradation.

Maternally expressed CDC25A regulates the first and second embryonic divisions

We next examined in more detail the role of CDC25A in early embryos. To determine whether CDC25A is required for the first embryonic division, we used maternal conditional knockout mice (*Cdc25a* F/F; Zp3-Cre; *Cdc25a* mKO) or control mice (*Cdc25a* F/F; *Cdc25a* WT), using *Zp3-Cre* to deplete the floxed *Cdc25a* allele specifically in oocytes. To produce *Cdc25a* mKO and *Cdc25a* WT embryos, *Cdc25a* mKO and *Cdc25a* WT females were mated with WT males.

We first determined *Cdc25a* mRNA abundance in *Cdc25a* WT and *Cdc25a* mKO in G2-phase zygotes (26 h post-hCG administration) and G2-phase two-cell embryos (42 and 46 h post-hCG administration). In *Cdc25a* WT embryos, *Cdc25a* mRNA abundance was high in zygotes in G2 at 26 h post-hCG administration and substantially decreased in two-cell embryos during the long G2 phase at 42 and 46 h after hCG administration. *Cdc25a* mRNA was virtually absent at all time points in *Cdc25a* mKO embryos (Fig 4A). Thus,

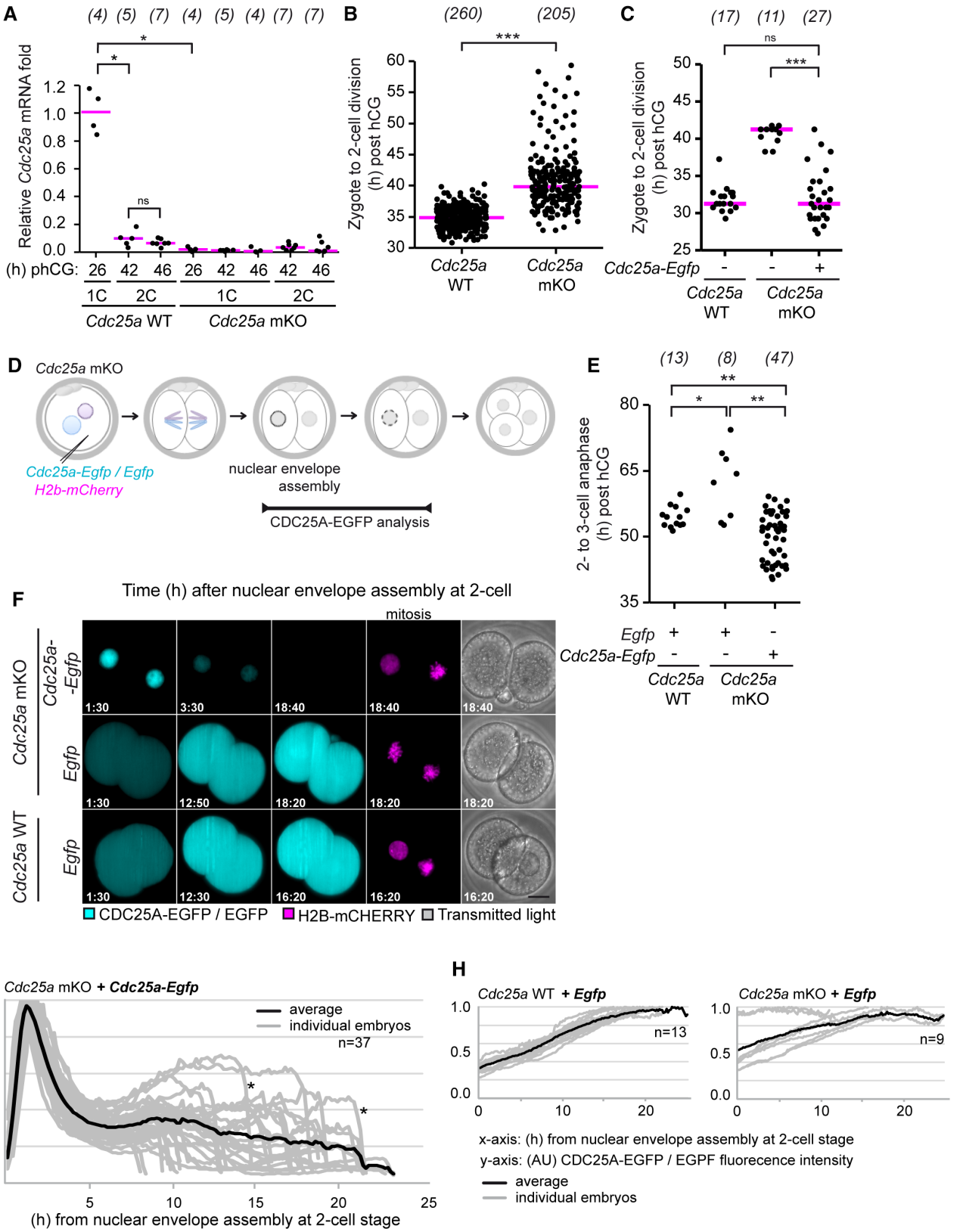
A
(4) (5) (7) (4) (5) (4) (7) (7)
Relative Cdc25a mRNA fold
(h) phCG: 26 42 46 26 42 46 42 46
1C 2C 1C 2C
Cdc25a WT
Cdc25a mKO
B
(260) (205)
Zygote to 2-cell division (h) post hCG
Cdc25a WT
Cdc25a mKO
C
(17) (11) (27)
Zygote to 2-cell division (h) post hCG
Cdc25a-Egfp
Cdc25a WT
Cdc25a mKO
D
Cdc25a mKO
Cdc25a-Egfp / Egfp
H2b-mCherry
nuclear envelope assembly
CDC25A-EGFP analysis
E
(13) (8) (47)
2- to 3-cell anaphase (h) post hCG
Egfp
Cdc25a-Egfp
Cdc25a WT
Cdc25a mKO
F
Time (h) after nuclear envelope assembly at 2-cell
mitosis
Cdc25a mKO
Cdc25a WT
Cdc25a-Egfp
Egfp
CDC25A-EGFP / EGFP
H2B-mCHERRY
Transmitted light
G
Cdc25a mKO + Cdc25a-Egfp
CDC25A-EGFP fluorescence intensity (AU)
average
individual embryos
n=37
(h) from nuclear envelope assembly at 2-cell stage
H
Cdc25a WT + Egfp
Cdc25a mKO + Egfp
n=13
n=9
x-axis: (h) from nuclear envelope assembly at 2-cell stage
y-axis: (AU) CDC25A-EGFP / EGPF fluorecence intensity
average
individual embryos

Figure 4.

Figure 4. Maternally expressed CDC25A regulates first and second embryonic division.

A Dot blot of relative average *Cdc25a* mRNA folds from individual *Cdc25a* WT and *Cdc25a* mKO embryos from 26 to 46 h post-hCG administration. 1C = one-cell, 2C = two-cell. The median is shown. The data are from one experiment with four *Cdc25a* WT and seven *Cdc25a* mKO mice treated individually. Data for each group are at least from 2 to 5 different mice. ns, non-significant, $P = 0.416793$, $^{*}P = 0.019964$ (26 h) and 0.030383 (42 h) (Mann–Whitney *U*-test, two-sided).

B Dot-plot of the division time (h) from bright-field time-lapse imaging of zygote to two-cell in *Cdc25a* WT and *Cdc25a* mKO embryos. The median is shown. The data were pooled from three independent experiments. $^{***}P = 0.00000$ (Mann–Whitney *U*-test, two-sided).

C Dot-plot of the division time (h) from bright-field time-lapse imaging from zygote to two-cell in *Cdc25a* WT, non-injected *Cdc25a* mKO and *Cdc25a* mKO embryos microinjected with *Cdc25a-Egfp* cRNA. The median is shown. The data are from one experiment. Strain background: C57J/BL6 background with small part CD-1 or CD-1 background with small part C57J/BL6. ns, non-significant, $P = 0.887045$, and $^{***}P = 0.00000$ (Mann–Whitney *U*-test, two-sided).

D Schematics of experimental design.

E Data from time-lapse light-sheet imaging (D) was used for quantification of the division time from two-cell to three-cell in *Cdc25a* WT embryos expressing EGFP, and *Cdc25a* mKO embryos expressing EGFP or CDC25A-EGFP from microinjected cRNAs. The data were pooled from four independent experiments. $^{*}P = 0.022409$, $^{**}P = 0.006582$ (vs. *Cdc25a* WT) and 0.002434 (vs. *Egfp*-microinjected *Cdc25a* mKO; Kolmogorov–Smirnov test, two-sided).

F Representative still images from time-lapse light-sheet imaging of preimplantation development of *Cdc25a* WT embryos expressing EGFP, and *Cdc25a* mKO embryos expressing EGFP or CDC25A-EGFP from microinjected cRNAs. Embryos were microinjected, as shown in (D). Embryos expressing CDC25A-EGFP or EGFP (cyan) and H2B-mCHERRY (magenta, chromosomes) are shown. Scale bar 20 μm. See also related Movie EV4 (*Cdc25A* mKO + CDC25A-EGFP, *Cdc25A* mKO + EGFP, and *Cdc25A* WT + EGFP).

G Line chart of fluorescence signal intensity of CDC25A-EGFP in *Cdc25a* mKO two-cell stage embryos from nuclear envelope assembly to nuclear envelope breakdown. Asterisk marks signal drop after nuclear envelope breakdown (not degradation).

H Line charts of fluorescence signal intensity of EGFP in *Cdc25a* WT or *Cdc25a* mKO two-cell stage embryos from nuclear envelope assembly to nuclear envelope breakdown.

Data information: The numbers in parentheses denote the number of embryos analyzed per group.

Cdc25a transcript is absent (or in very low abundance) during the long G2 phase in two-cell embryos.

Because results described above suggested a role for CDC25A in regulating cell cycle progression, we examined the timing of cell division of *Cdc25a* mKO zygotes. Bright-field time-lapse imaging revealed a significant delay in cleavage of zygotes of *Cdc25a* mKO embryos (Fig 4B) that was rescued by *Cdc25a-Egfp* cRNA microinjection (Fig 4C). We then monitored the CDC25A-EGFP signal in *Cdc25a mKO* two-cell embryos from nuclear envelope assembly to NEBD (Fig 4D–F; Movie EV4). Similarly, *Cdc25a* mKO embryos showed a delay in the second mitosis, and injection with *Cdc25a-Egfp* cRNA rescued the delay (Fig 4E). Notably, the rescued *Cdc25a* mKO embryos showed a greater variability in the timing of the second embryonic mitosis, with a proportion showing the second embryonic mitosis earlier than the *Cdc25a* WT embryos (Fig 4E). A portion of the *Cdc25a* mKO embryos showed WT-like timing of the second anaphase, which could have reflected a CDC25A-EGFP concentration similar to that of wild-type CDC25A in WT embryos. In these embryos, the CDC25A-EGFP signal rapidly increased with a peak corresponding to the time of the G1/S transition, followed by CDC25A-EGFP degradation corresponding to the time of S phase progression (Fig 4G). Most embryos then showed a slight CDC25A-EGFP signal increase around 6–10 h post-nuclear envelope assembly, followed by a rapid signal decrease after NEBD during mitotic entry or by a slight signal decrease. The signal from EGFP alone increased gradually from the nuclear envelope assembly until NEBD, suggesting that changes in CDC25A-EGFP intensity are not due to selective translation or degradation of the EGFP moiety of the fusion protein (Fig 4G and H). Thus, in two-cell embryos, CDC25A is degraded during S phase progression and remains lower thereafter.

Having confirmed that CHK1 regulates entry to mitosis by controlling CDC25A degradation in mouse embryos (Fig 3D and G), we were interested in testing whether CHK1 inhibition affects the timing of mitosis in *Cdc25a* mKO embryos. To do so, we isolated zygotes from WT and *Cdc25a* mKO mice and monitored the blastocyst development in the presence of 250 nM CHIR-124 using bright-field time-lapse imaging. Although the CHK1 inhibition slightly but significantly accelerated the first division in WT embryos, the timing of the first mitosis was not affected in *Cdc25a* mKO (Appendix Fig S3A). As confirmed above (Fig 4B, C, and E), *Cdc25a* mKO embryos showed a delay in the first and second mitosis. However, treatment with CHIR-124 does not accelerate this timing of second mitosis in WT, as well as *Cdc25a* mKO embryos (Appendix Fig S3B). Taken together, these results indicate that CDC25A is essential for regulating cell cycle progression of zygotes and two-cell embryos.

Maternal CHK1 regulates chromosome segregation, and its absence causes genome fragmentation

CHK1 is a critical DDR kinase (Takai *et al*, 2000). Its depletion causes chromosome instability in eight-cell embryos (Ruth *et al*, 2021) and DNA damage, premature mitosis, chromosome fragmentation, and micronuclei formation in cell lines (Hoffelder *et al*, 2004; Niida *et al*, 2005; Durkin *et al*, 2006; Peddibhotla *et al*, 2009; Dandoulaki *et al*, 2018). Therefore, we next examined chromosome stability in *Chk1* mKO embryos using long-term time-lapse imaging on a light-sheet microscope and visualized chromosomes (Fig 5A).

In the first division (zygote to two-cell stage), anaphase was accelerated by 1 h in *Chk1* mKO embryos compared to *Chk1* WT (Fig EV4A; Movie EV5). Also, *Chk1* mKO embryos showed a slight but non-significant increase in chromosome segregation errors during the first anaphase (Fig 5B and C; Movie EV5). The acceleration of anaphase in *Chk1* mKO embryos was more pronounced at the two- to three-cell division (Fig EV4B), and by the four-cell stage, nearly 80% displayed chromosome segregation errors compared to 20% of control embryos (and more pronounced in *Chk1* mKO *class I* than *Chk1* mKO *class II* embryos (Figs 5D and EV4C)). In individual *Chk1* mKO embryos, only mild segregation errors were observed during the first anaphase (Fig EV4D; Movie EV5). The chromosome segregation errors in later stages were lagging chromosomes, anaphase bridges, and

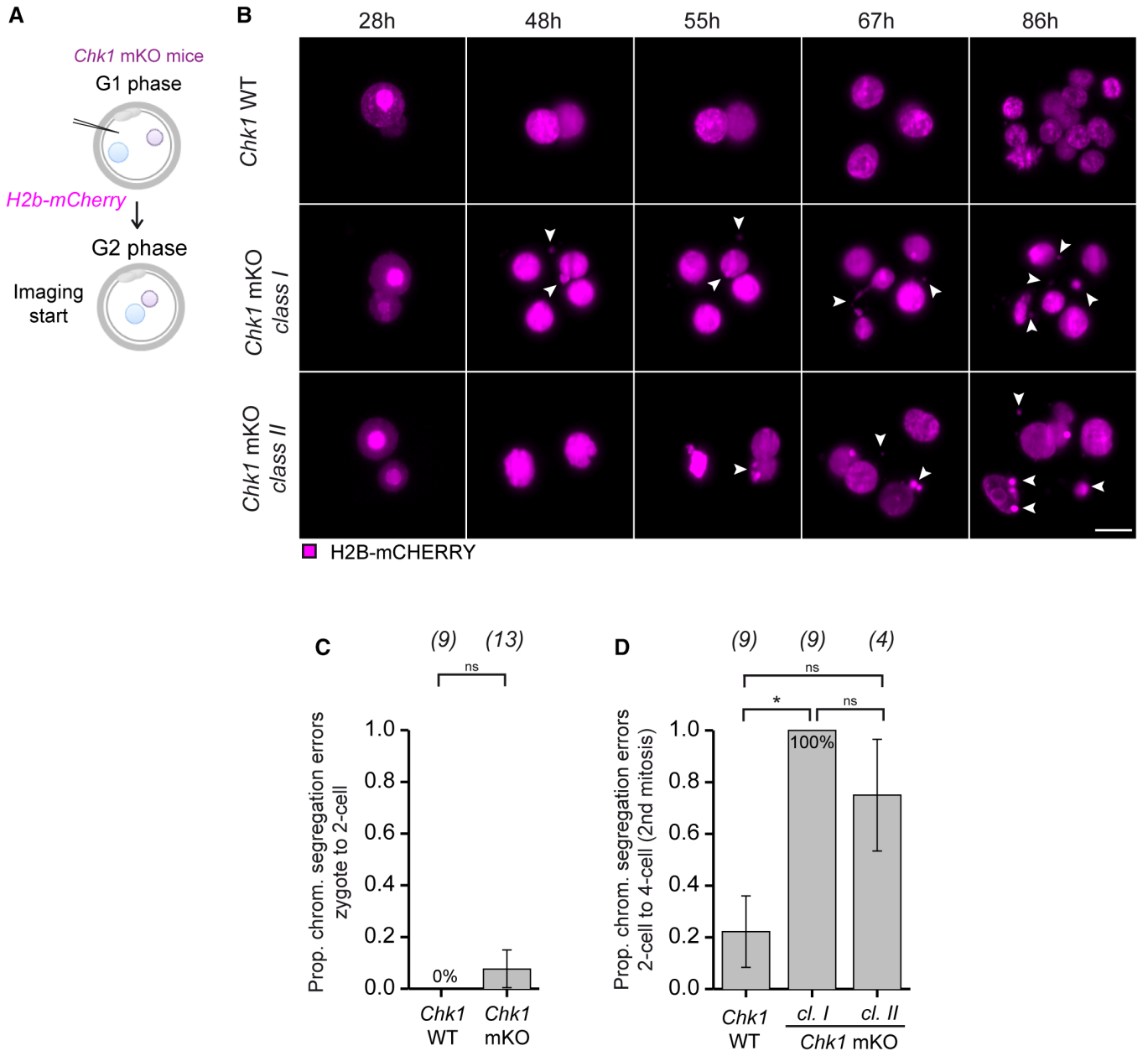

Figure 5. Massive genome fragmentation in *Chk1* mKO embryos is caused by chromosome segregation errors during the second mitosis.

A Schematic of the experimental procedure.

B Representative still images from time-lapse light-sheet imaging of *Chk1* WT, *Chk1* mKO *class I*, and *Chk1* mKO *class II* embryos from 28 to 86 h post-hCG administration. Embryos were microinjected, as shown in (A). Embryos expressing H2B-mCHERRY (magenta, chromosomes) are shown. Time points are relative to time post-hCG administration (h). Arrowheads mark genome fragmentation. Scale bar 20 μm. See also related Movie EV5 (*Chk1* WT, *Chk1* mKO *class I*, and *Chk1* mKO *class II*).

C, D Data from time-lapse light-sheet imaging (B) was used to quantify the percentage of filmed embryos with chromosome segregation errors in the first embryonic division from zygote to two-cell stage (C) and in the second embryonic division from two-cell to three-cell stage and three-cell stage to four-cell stage (D). Chromosome segregation errors were counted if observed in at least one of these divisions. The numbers in brackets denote the number of analyzed embryos per genotype. The data were pooled from two independent experiments. Error bars denote the standard error of proportion. ns, non-significant, and *$P = 0.023$ (Fisher's exact test).

genome fragmentation (Fig EV4E and F; Movie EV6). We also observed these segregation errors in *Chk1* mKO embryos that showed WT timing of the initial embryonic divisions. Thus, CHK1 is essential for genome integrity during the initial embryonic divisions after fertilization.

Preventing zygotic genome activation by α-amanitin does not rescue genome fragmentation in *Chk1 mKO* embryos

Next, we sought to understand the basis for the chromosome segregation errors after *Chk1* depletion. CHK1 is a component of the

replication stress response, which can be triggered by transcription–replication collisions (Blythe & Wieschaus, 2015; Sollier & Cimprich, 2015; Barroso *et al*, 2019; Lam *et al*, 2020). Transcriptional activity in mouse two-cell embryos is high because of the major phase of genome activation (Knowland & Graham, 1972; Flach *et al*, 1982; Bolton *et al*, 1984; Aoki *et al*, 1997). Therefore, we asked whether preventing zygotic genome activation would suppress chromosome segregation errors in *Chk1* mKO embryos (Figs 5D and EV2G).

We inhibited RNA polymerase II and III by culturing zygotes in α-amanitin (24 μg/ml) from 26 h after hCG administration (Fig 6A). At this time, the majority of embryos have completed the first S phase (Rambhatla & Latham, 1995; Qiu *et al*, 2003; Zeng & Schultz, 2005) but have not yet initiated major zygotic genome activation (Aoki *et al*, 1997; Hamatani *et al*, 2004). α-amanitin treatment did not rescue the premature division of *Chk1* mKO embryos (Fig EV5A). Whereas α-amanitin treatment led to a robust two-cell stage block in *Chk1* WT embryos even at 68 h (Fig 6B and C), a robust two-cell stage block depended on *Chk1* because 62% of the α-amanitin-treated *Chk1* mKO embryos progressed to the three- or four-cell stage at 68 h before arresting (Fig 6B and C). These embryos remained in the two- or three-/four-cell stage until 114 h post-hCG stimulation, when 69% of DMSO-treated *Chk1* WT developed into blastocyst stage (Fig EV5B and C). Increased genome fragmentation, as assayed by DAPI staining, was observed in four-cell *Chk1* mKO embryos cultured in the presence of α-amanitin (24 μg/ml) as well as DMSO (Fig 6D) from 26 to 68 h post-hCG administration (Fig 6E and F). Thus, when major genome activation is inhibited in *Chk1* mKO embryos by α-amanitin, maintaining of two-cell stage block depends on CHK1 activity, but genome fragmentation is not dependent upon α-amanitin treatment.

The long G2 phase in two-cell embryos is necessary for genome integrity

We suspected that the cause for the high incidence of chromosome segregation errors after *Chk1* depletion during the second division was due to premature mitosis due to a shortened G2 phase. Accordingly, we forced *H2b-Egfp* transgenic embryos into premature mitosis by WEE/MYT pharmacological inhibition (Ferencova *et al*, 2022) at 44 h post-hCG administration (Fig 7A). At this time, 92% of WT embryos were in G2 because we did not detect DNA replication following an EdU pulse (Appendix Fig S1F and G). WEE/MYT-inhibited two-cell embryos entered mitosis 7 h earlier than controls (Fig 7B), and was accompanied by segregation errors in 66% of the embryos as well as an extended M phase (1.8 h compared to 0.8 h in WT; Fig 7C and D). Thus, shortening the G2 phase in two-cell embryos by inhibiting WEE/MYT is associated with genome fragmentation.

The G2/M transition is regulated by CDK1 kinase. Therefore, we asked whether the DNA damage and chromosome segregation errors in *Chk1* mKO embryos are a consequence of premature CDK1 activation. To this end, we partially inhibited CDK1 in two-cell embryos with 2.5 μM RO-3306 and analyzed DNA integrity in four-cell embryos. Partially CDK1-inhibited *Chk1* mKO embryos showed reduced genome fragmentation compared to DMSO-treated *Chk1* mKO embryos (Fig 7E). The incidence of genome fragmentation in the *Chk1* mKO embryos exposed to partial CDK1 inhibition was similar to that in *Chk1* WT embryos (Fig 7E and F). Taken together, these findings show that partial inhibition of CDK1 rescues both M phase timing and genome fragmentation in two-cell *Chk1* mKO. We infer that CHK1 restrains CDK1 activity by promoting CDC25A degradation to regulate cell cycle progression and protect genome integrity in two-cell embryos (Fig 7G).

Discussion

Cell cycle progression during early development is accompanied by shortening and/or lengthening of G1 or G2 compared to somatic cells. For *Drosophila*, *Xenopus*, zebrafish, and mammals, fertilization is followed by a long G1 (Hörmanseder *et al*, 2013), in contrast to a short or absent G1 before the major phase of genome activation (Fig 2; Artus & Cohen-Tannoudji, 2008; Palmer & Kaldis, 2016). Genome activation depends on lengthening G1 or G2 (Flach *et al*, 1982; Newport & Kirschner, 1982; Foe & Alberts, 1983; Zamir *et al*, 1997; Carson & Kallen, 2021).

In *Xenopus*, WEE1-to-CDC25 ratio is critical for the difference in length of the first and second cell division (Tsai *et al*, 2014). On the other hand, regulation of the long G2 phase in mammalian embryos is poorly understood, and it was thought that the G2/M depended on transcription during genome activation (Flach *et al*, 1982). Results reported here show that the G2/M transition in mouse two-cell embryos is *Chk1* dependent, where CHK1 prevents premature mitosis by restraining CDK1 activity by inducing CDC25A degradation. Thus, we propose that the long G2 phase is normally maintained by the absence of CDC25A until CDK1 is activated by its newly transcribed activators after genome activation (Fig 7G). In support of this model is that maternal *Chk1* depletion caused decrease in percentage of G2 zygotes (Fig EV2D) and shortened the length of G2 in 2-cell embryos (Fig 2), with a premature mitosis following in both cases (Fig 1); premature mitotic entry in two-cell *Chk1* mKO embryos results from CDC25A protein stabilization (Fig 3D and G) and CDC25A overexpression induces premature mitosis (Fig EV3C and D). Generation of newly transcribed CDK1 activators is consistent with an increase in transcript abundance of mitotic activators such as CDK1, CDK2, and cyclins D1-3, E1, A2, and CDC25C from the zygote to the two-cell stage (Abe *et al*, 2018). Experiments with α-amanitin (Fig 6) confirm our hypothesis that CHK1 inhibits the second mitosis entry until the transcription of a sufficient amount of *Cdk1* and CDK1 activators (*Ccna2*, *Cdc25c*; Zeng *et al*, 2004; Park *et al*, 2013; Abe *et al*, 2018). The transcription of these CDK1 activators is required because of the low amount of natural *Cdc25a* mRNA (Fig 4A) and possibly the absence of CDC25A protein (Fig 3C). The low levels of *Cdc25a* mRNA in two-cell embryos may therefore become rate limiting for cell cycle progression, which is delayed until, for example, *Cdc25c* mRNA levels increase in the major genome activation (Zeng *et al*, 2004; Xie *et al*, 2010; Park *et al*, 2013). In support of this model also is that CDC25A-EGFP is degraded during the time similar to S-phase timing in WT two-cell embryos (Fig 3C) and CDK1 inhibition rescues the G2 duration and the timing of M phase in *Chk1* mKO embryos (Fig 3A). This model is consistent with others. *Chk1* depletion causes aberrant embryonic development in mice (Liu *et al*, 2000; Takai *et al*, 2000). CHK1 inhibition causes premature mitosis in both mouse (Ju *et al*, 2020) and human (Palmerola *et al*, 2022) zygotes.

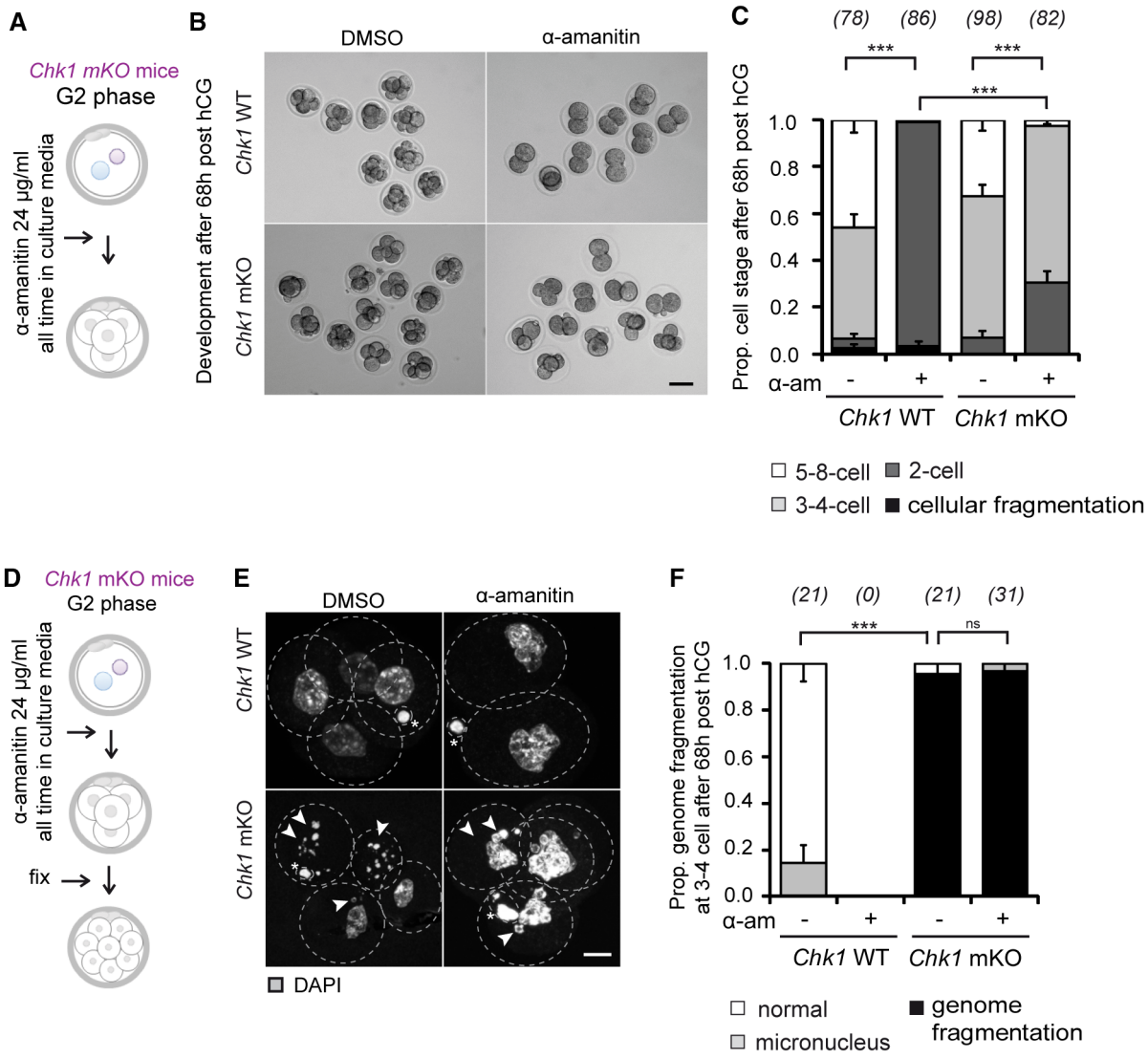

Figure 6. DNA damage and chromosome segregation errors in *Chk1* mKO embryos are not transcription dependent.

A Schematic depiction of the experimental procedure.

B Representative images from developmental analysis of *Chk1* WT and *Chk1* mKO embryos treated with DMSO or α-amanitin (24 µg/ml). Embryos were scanned at 68 h post-hCG administration. Strain background: CD-1 with small part C57J/BL6 and C57J/BL6 with small part CD-1. Scale bar 60 µm.

C Proportion of developmental stages of embryos (as shown in B) at 68 h post-hCG administration. The data were pooled from three independent experiments. Error bars denote standard error of proportion. ***P = 0.00000 (Cochran–Armitage trend test, two-sided).

D Schematic depiction of the experimental procedure.

E Representative images from genome integrity analysis of *Chk1* WT and *Chk1* mKO embryos treated with DMSO or α-amanitin (24 µg/ml). The embryos were scanned at 68 h post-hCG administration. Embryos stained with DAPI (gray, chromatin) are shown. A dashed line indicates blastomeres outlines as seen in a bright field. Arrowheads mark genome fragmentation. Asterisk marks polar bodies. Strain background: CD-1 with small part C57J/BL6 and C57J/BL6 with small part CD-1. Scale bar 10 µm.

F Proportion of genome fragmentation of embryos (as shown in E). Only three- to four-cell stages were analyzed. Note that all α-amanitin-treated *Chk1* WT embryos were arrested in the two-cell stage. The data were pooled from two independent experiments. Error bars denote standard error of proportion. ns, non-significant, P = 0.46453, and ***P = 0.00000 (Cochran–Armitage trend test, two-sided).

Data information: The numbers in parentheses denote the number of analyzed embryos per group.

CHK1 kinase activity itself is necessary for early embryos (Muralidharan *et al*, 2020). It is also consistent with other studies in mice (Lam *et al*, 2004; Niida *et al*, 2005; Peddibhotla *et al*, 2009; Fishler *et al*, 2010; Ruth *et al*, 2021), humans (Niida *et al*, 2005; Syljuåsen *et al*, 2005; Durkin *et al*, 2006; Branigan *et al*, 2021), and other species (Zachos *et al*, 2003, 2005, 2007).

Although CHK1 kinase does not participate in completing the main phase of DNA replication (Fig EV2), we find that it is essential

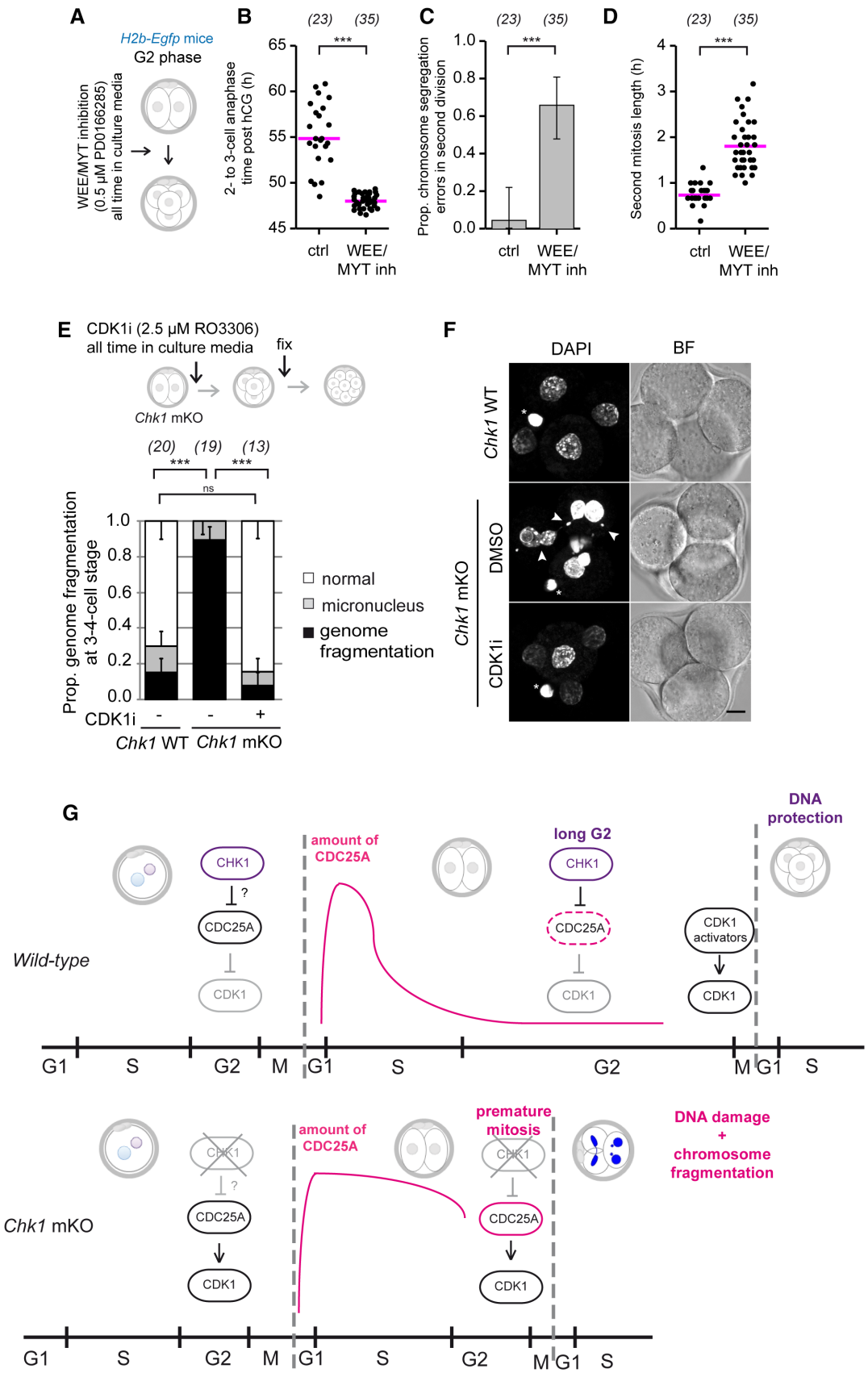

Figure 7.

Figure 7. CHK1 is necessary for genome integrity during long G2 in two-cell stage mouse embryos.

A Schematic depiction of the experimental procedure.

B–D Data from time-lapse light-sheet imaging of embryos from *H2b-Egfp* transgenic mice after WEE/MYT kinases inhibition (as shown in A) at 44 h post-hCG administration (G2 phase) were used to quantify the initiation of anaphase (h) from two-cell to three-cell stage embryos (B), and length of mitosis (h) in two-cell to three-cell stage embryos (D). The data were pooled from two independent experiments. The median is shown. ***P = 0.00000 (Aspin–Welch unequal-variance T-test). (C) Data from time-lapse light-sheet imaging of embryos from *H2b-Egfp* transgenic mice after WEE/MYT kinases inhibition (as shown in A) at 44 h post-hCG administration (G2 phase) were used to quantify the percentage of filmed embryos with chromosome segregation errors. Error bars denote the 95% confidence interval. ***P = 0.00000 (Fisher's exact test, two-sided).

E Genome integrity analysis of *Chk1* WT, DMSO-treated *Chk1* mKO, and RO3306-treated *Chk1* mKO (CDK1 inhibition) within 3 h after two-cell division. The embryos were scored at 60 h post-hCG administration, and only three- to four-cell stage embryos were analyzed. The data are from one experiment with four groups of different mice of *Chk1* mKO and one group of *Chk1* WT. Error bars denote standard error of proportion. ns, non-significant, P = 0.37134, and ***P = 0.00000 (Cochran–Armitage trend test, two-sided).

F Representative images from genome integrity analysis of embryos (E). The embryos were scanned at 60 h post-hCG administration. Embryos stained with DAPI (gray, chromatin) are shown. Arrowheads mark genome fragmentation. Asterisk marks polar bodies. BF, bright-field. Scale bar 20 μm.

G Model of cell cycle regulation and genome integrity protection by CHK1 in early mouse embryos. In wild-type mouse embryous, active CHK1 (shown in purple) restrains CDK1 activity (gray) by promoting CDC25A degradation (dashed magenta line) to regulate cell cycle progression and protect genome integrity in two-cell embryos. CDK1 is activated (black) by its newly transcribed activators after genome activation. The absence of CHK1 (crossed) causes premature CDK1 kinase activation (black) due to stabilization of CDC25A phosphatase (solid magenta line), which leads to premature mitosis and chromosome fragmentation. The magenta curve represents the amount of CDC25A protein in individual cell cycle phases in two-cell stage wild-type and *Chk1* mKO embryos.

Data information: The numbers in parentheses denote the number of analyzed embryos per group.

to preserve genome integrity by maintaining a long G2 phase in two-cell mouse embryos by restraining CDK1 activity due to CDC25A degradation (Fig 7G). This conclusion is based on a conditional gene knockout approach and pharmacological inhibitors, noting that it is formally possible that non-specific effects of the inhibitors could contribute to the observed phenotype. Minimizing this possibility is that RO-3306 treatment inhibits resumption of meiosis in mouse oocytes (Fig EV3A), thereby showing the efficiency of CDK1 inhibition by RO-3306. In addition, we previously showed that PD0166285 treatment rescues milrinone-induced prophase I arrest in mouse oocytes (Ferencova *et al*, 2022), indicating an effective inhibition of WEE/MYT kinases. The absence of CHK1 in mouse embryos phenocopied the effect of CHIR-124 on blastocyst development (Fig EV1F) and timing of the first embryonic division (Appendix Fig S3A) but not on the timing of the second embryonic division (Appendix Fig S3B), a difference likely caused by the lower specificity and/or efficiency of the inhibitor.

There are evolutionary conserved features and differences in CHK1's role in regulating cell cycle length in embryonic development. In non-mammalian models, genome activation is preceded by 9–14 rapid cell cycle divisions (Dalle Nogare *et al*, 2009; Collart *et al*, 2013; Blythe & Wieschaus, 2015), during which ATR-CHK1 is prevented from recognizing replication stress (Sibon *et al*, 1997; Shimuta *et al*, 2002; Holway *et al*, 2006; Zhang *et al*, 2014; Blythe & Wieschaus, 2015). At the time of genome activation, CHK1 causes CDC25A degradation in both zebrafish (Dalle Nogare *et al*, 2009; Zhang *et al*, 2014), *Drosophila* (Deneke *et al*, 2016), and *Xenopus* (Shimuta *et al*, 2002; Petrus *et al*, 2004), as in mouse reported here (Fig 3). In *Xenopus*, CHK1 inhibits replication initiation factor DRF1, thus blocking early embryo cell cycle progression (Collart *et al*, 2017). Whether CHK1 in mammals regulates other CDKs and CDC25s during genome activation during the maternal-to-zygotic transition warrants further investigation, noting that CHK1 overexpression in *Xenopus* egg extracts causes CDC25A degradation without affecting CDC25C levels (Hartley *et al*, 1996; Petrus *et al*, 2004) and inhibiting CDC25A and CDK1 but not CDK2 causes lengthening of the long G2 during genome activation in zebrafish (Dalle Nogare *et al*, 2009).

Our results are consistent with a step-wise increasing activation of CDK1 in early embryos such that by reaching certain thresholds during cell cycle progression-specific cell cycle transitions/phases (G1/S transition, S phase progression, G2 length, and mitotic entry) occur (Fig 2; Niida *et al*, 2005; Lemmens *et al*, 2018; Branigan *et al*, 2021; Suski *et al*, 2022). This model implies that for a premature mitotic entry from early or middle S phase, CDK1 activity needs to be increased more than for a premature mitotic entry from the late S or G2 phase (Pomerening *et al*, 2003; Sha *et al*, 2003). Consistent with this proposal is that CHK1 depletion/inhibition or CDC25A-EGFP overexpression alone causes premature mitotic entry only from the late S or G2 phase (Figs 2 and EV3F; Niida *et al*, 2005; Lemmens *et al*, 2018; Branigan *et al*, 2021). For premature mitotic entry from the early or middle S phase, (i) a concomitant *Chk1* depletion and CDC25A-EGFP co-expression (Figs 3D and EV3F), or (ii) separate WEE/MYT kinase inhibition (Fig 7B and Appendix Fig S1C) is required.

The extent to which CHK1 regulates replication completion is not fully understood. Although *Chk1* mKO *class I* embryos exhibit premature mitotic entry after finishing the main period of S phase progression (Fig 2), this observation does not necessarily mean they completed replication. The transition to G2 is set by a low threshold of origin firing (Zonderland *et al*, 2022), but in some cases, replication can continue during G2 phase (Mocanu *et al*, 2022; Palmerola *et al*, 2022). This finding is consistent with other studies (Lam *et al*, 2004; Branigan *et al*, 2021), where *Chk1* depletion or inhibition causes premature mitosis in cells with only mildly, but not severely, underreplicated DNA.

CHK1 is activated after replication stress in somatic cells and early embryos (Lam *et al*, 2004; Syljuåsen *et al*, 2005; Zachos *et al*, 2005; González Besteiro & Gottifredi, 2015; Lemmens *et al*, 2018; Michelena *et al*, 2019; Moiseeva *et al*, 2019; Muralidharan *et al*, 2020; Lebrec *et al*, 2022; Palmerola *et al*, 2022). Replication stress signaling is usually orchestrated by ATR kinase (Eykelenboom *et al*, 2013; Saldivar *et al*, 2018). However, the role of ATR in early embryos does not seem as prominent as CHK1. *Atr* germ-line KO embryos show better development than *Chk1* germ-line KO embryos (Brown & Baltimore, 2000; Liu *et al*, 2000; Takai *et al*, 2000).

Disrupting CHK1-CDC25A-CDK1 regulation results in DNA damage (Fig EV2G and I), chromosome segregation errors (Figs 5B and D, and EV4C–F), aneuploidies, and infertility (Ruth *et al*, 2021). These findings are consistent with studies in mice (Lam *et al*, 2004; Niida *et al*, 2005; Peddibhotla *et al*, 2009; Fishler *et al*, 2010; Ruth *et al*, 2021), humans (Niida *et al*, 2005; Syljuåsen *et al*, 2005; Durkin *et al*, 2006; Branigan *et al*, 2021), and other species (Zachos *et al*, 2003, 2005, 2007). We observed, however, that the gross DNA damage and chromosome segregation errors after *Chk1* depletion occur only in two-cell embryos (Figs 5D and EV2G) and not in zygotes (Figs 5C and EV2C). This finding contrasts with human zygotes, where CHK1 inhibition causes both DNA damage and segregation errors in nine of nine embryos, noting that development of human embryos is more error prone (Vanneste *et al*, 2009; Cavazza *et al*, 2021; Currie *et al*, 2022; Palmerola *et al*, 2022) than inbred mice (Bolton *et al*, 2016; Mashiko *et al*, 2020). These observations suggest an evolutionary difference (Svoboda, 2018), where zygotes from inbred mice are more efficient in protecting their DNA integrity.

Infertility rates worldwide are increasing (Carson & Kallen, 2021; Gruhn & Hoffmann, 2022). About 50% of human embryos do not develop to the blastocyst stage due to a high incidence of aneuploidy (preprint: McCoy *et al*, 2022). Also, almost 95% of human arrested embryos show chromosome segregation errors (preprint: McCoy *et al*, 2022), and even in blastocysts, 20% show mosaicism when disaggregated (Capalbo *et al*, 2021) or 30% when a biopsy is analyzed (preprint: McCoy *et al*, 2022). There is increasing evidence that some of these aneuploidies are of mitotic (embryonic) origin (Vanneste *et al*, 2009; preprint: McCoy *et al*, 2022). It was recently found that novel genetic mutations in *Chk1* are responsible for zygotic arrest causing infertility in humans (Zhang *et al*, 2021; Chen *et al*, 2022). Results reported here using a mouse model implicate CHK1-CDC25A-CDK1 regulation as another mechanism whose dysregulation could contribute to human infertility.

Materials and Methods

Animal use and *Chk1 mKO* generation

Mice were handled and experiments were conducted accordingly to the guidelines of the Expert Committee for the Approval of Projects of Experiments on Animals of the Academy of Sciences of the Czech Republic (no. 43-2015). Mice were housed at the Institute of Animal Physiology and Genetics of the Czech Academy of Sciences in Libechov, Czech Republic. Mice were housed under conditions of a 12 h day–night cycle at 22°C (± 2°C) and had access to food and water *ad libitum*.

The *Chk1* mKO embryos were created as in Ruth *et al* (2021) by crossing mice carrying a Cre-recombinase expressed from the oocyte-specific *Zp3* promoter (Lewandoski *et al*, 1997) to mice with floxed *Chk1* alleles (Lam *et al*, 2004). All experiments were conducted using littermates. The mice were on CD-1 background with a small part of C57J/BL6 if not noted otherwise in Figure legends.

The *Cdc25a* mKO embryos were created by crossing mice carrying a Cre-recombinase expressed from the oocyte-specific *Zp3* promoter (Lewandoski *et al*, 1997) to mice with floxed *Cdc25a* alleles (Lee *et al*, 2009). All experiments were conducted using littermates. The mice were on C57J/BL6 background with a small contribution of CD-1 if not noted otherwise in Figure legends.

H2b-Egfp mice were on CD-1 background (Mayer *et al*, 2016).

WT strain of mice was either CD-1 (ICR) or C57J/BL6.

Genotyping

Animals were genotyped two times, initially upon weaning and again after experimental procedures were carried out.

Chk1 mKO genotyping was performed by PCR analysis using the following primers for mKO *Chk1(Zp3-Cre)*: CHK1F1 (5′-ACC TGC CCG CAA CTC CCT TTC-3′), CHK1R1(5′-CCA TGA CTC CAA GCA CAG CGA-3′), Cre_low (5′-TAT TCG GAT CAT CAG CTA-3′), and Cre_up (5′-GGT GGG AGA ATG TTA ATC-3′). The sizes of products were 318 bp for WT and 380 bp for *lox/lox* transgene. The size of the *Zp3*-Cre transgene was 139 bp. The *Taq* 2× Master Mix was used for genotyping (NEB, # M0270L).

Cdc25a mKO genotyping was performed by PCR analysis using the following primers for *Cdc25a* mKO *(Zp3-Cre)*: oIMR9611: (CAG AGC CTG AAG TCC TGT GAA GG), oIMR9612: (CTG GGT AGT GTA GTT CCT ACA GCG), Cre_low: (5′-TAT TCG GAT CAT CAG CTA-3′), and Cre_up: (5′-GGT GGG AGA ATG TTA ATC-3′). The sizes of products were 222 bp for WT and 270 bp for *lox/lox* transgene. The size of the *Zp3*-Cre transgene was 139 bp. The *Taq* 2× Master Mix was used for genotyping (NEB, # M0270L).

Chk1 mKO embryo genotyping (Fig EV1J) was performed by nested PCR analysis using the following primers. For the first nested PCR reaction: *Chk1*_FWD_01 (5′-TTTTGGCGGGAAAAGCTGTG-3′) and *Chk1*_REV_01 (5′-CTATGGCCCGCTTCATGTCT-3′). For the second nested PCR reaction: *Chk1*_FWD_02 (5′-GACGGAGGA-CAAACGTGGAA-3′) and *Chk1*_REV_01. The sizes of products after the second PCR were 2,218 bp for WT with LoxP sites and 398 bp after Cre-induced recombination. The Taq 2× Master Mix was used for genotyping (NEB, # M0270L).

Superovulation and embryo handling

Mice, ranging from 3–6 months of age, were stimulated with 5 IU of PMSG (HOR-272, ProSpec-Tany TechnoGene), and after 44 h with 5 IU of hCG (Ovitrelle, Merck) and then mated with a WT CD-1 male. The females were sacrificed by cervical dislocation after 18 h in accordance with the guidelines of the ethics committee.

The oviducts were placed in M2 medium (M7167, Merck), and the ovulated MII oocytes and zygotes were collected from torn ampullae. The cumulus mass containing the MII oocytes and zygotes was transferred to a drop of M2 medium containing 300 μg/ml hyaluronidase (H4272, Merck) to release the cumulus cells. The MII oocytes and zygotes were cultured in EmbryoMax KSOM medium (MR-106-D, Merck) at 37°C with 5% CO_2 in an atmosphere of air. For live-cell imaging, embryos were cultured in global® (LGGG-020, Origio) supplied with 1 mg/ml BSA. Only zygotes with visible pronuclei were used for experiments.

The temporal information about embryo development is given in (h) post-hCG administration, as this is the last exact time point in mating with males.

Oocyte handling

For oocyte collection, mice were stimulated with 5 IU of PMSG (HOR-272, ProSpec-Tany TechnoGene), and the germinal vesicle (GV)-stage oocytes were collected in M2 medium supplied with 2.5 μM milrinone (M4659, Merck) to prevent resumption of meiosis. The oocytes were cultured in minimum essential medium (MEM, Merck, M4655) containing 1.14 mM sodium pyruvate (Merck, P4562), 4 mg/ml bovine serum albumin (BSA, Merck, A3311), and penicillin–streptomycin (75 U/ml-60 μg/ml, Merck, P7794, S1277), and incubated at 37°C in 5% CO_2 in an atmosphere of air.

Inhibitors

All used inhibitors were diluted in DMSO (Merck, D2650). The concentrations used were as follows: CHK1 inhibitor (CHIR-124) 250 nM, CDK1 inhibitor (RO-3306) 2.5 μM, and WEE/MYT inhibitor (PD0166285) 0.5 μM (Ferencova *et al*, 2022).

Plasmid preparation

The pCMV-Sport6-Chk1 plasmid containing mouse *Chk1* cDNA (NM_007691.5, from nucleotides 117 to 1,541) and the pBSK-EGFP plasmid were kindly provided by Martin Anger, IAPG CAS, Libechov and CEITEC, Brno, Czech Republic. *Chk1* coding sequence was cloned into pBSK-EGFP using SpeI restriction sites to create pBSK-EGFP-Chk1 plasmid. To create pYX-Chk1 plasmid, EGFP sequence was replaced by *Chk1* coding sequence in pYX-EGFP (Blengini *et al*, 2021) using SpeI restriction sites.

To create a *Cdt1* sensor suitable for mouse oocytes and embryos, we modified a mCherry-hCdt1(1-100)Cy(−)pcDNA3 plasmid (RIKEN BRC DNA Bank; Sakaue-Sawano *et al*, 2017). We performed codon optimization using the IDT Codon Optimization Tool (Integrated DNA Technologies). The modified *mCdt1* sequence was synthesized (Integrated DNA Technologies) and cloned into pYX-EYFP (Blengini *et al*, 2021) using SpeI restriction sites to create pYX-EYFP-*mCdt1* plasmid for transcription of *mCdt1*-EYFP sensor.

Other plasmids for *in vitro* transcription were already described —pBSK-H2B-mCherry (Kitajima *et al*, 2011), pBSK-EGFP-Cdc25A (Solc *et al*, 2008), and pXY-EGFP (Saskova *et al*, 2008; Blengini *et al*, 2021).

cRNA production and microinjection

For cRNA preparation, plasmids were linearized by AscI (pBSK vector) or SfiI (pYX vector) and purified by NucleoSpin Gel and PCR Clean-up kit (Macherey-Nagel, #740609). cRNA was produced by *in vitro* transcription using mMessage mMachine™ T3 kit (Ambion, #1348). *Chk1-Egfp*, *Chk1*, *Egfp*, and *Cdc25a-Egfp* cRNAs were polyadenylated using the Poly(A) Tailing Kit (Ambion, #AM1350) according to manufacturer's protocols. cRNAs were purified using RNeasy Mini Kit (Qiagen, #74104) and stored at −80°C. The oocytes or embryos were microinjected with ~10 pl of a cRNA solution (35 ng/μl *H2b-mCherry*, 10 ng/μl *Egfp-Chk1*, or *Egfp*) alone for *Chk1 mKO* rescue in Fig 1G, 300 ng/μl *Chk1* alone for immunoblotting, 50, 75, or 100 ng/μl *Egfp-Cdc25a*, and 50 ng/μl *Egfp* alone.

Single-oocyte/embryo real-time qPCR

Expression level of *Cdc25a* mRNA was measured by RT–qPCR using FastLane Cell SYBR Green kit (Qiagen, #216213) using CFX96 Touch Real-Time PCR Detection System, Bio-Rad. Single oocytes or embryos were directly used as a substrate for single-step RT–qPCR without mRNA purification. External *Gfp* mRNA (0.04 pg *Gfp* mRNA per oocyte/embryo) was added to lysed oocytes or embryos to serve as a control for RNA quantification and normalization of RT–qPCR data. The following gene-specific primers were used: *Cdc25a* primers located at 5′ end of mRNA (AATAACAGCAGTCTACAG and TTCAAGGTTTTCTTTACTG); *Cdc25a* primers located at 3′ end of mRNA (AGAACCCTATTGTGCCTACTG and TACTCATTGCCGAGCCTATC); and *Gfp* primers (TTCAAGATCCGCCACAAC and GACTGGGTGCTCAGGTAG). The following single-step RT–qPCR protocols were used (modified from Solc *et al*, 2008): *Cdc25a* 5′ end: 1. 50°C 30 min, 2. 95°C 15 min, 3. 94°C 15 s, 4. 52°C 30 s, 5. 72°C 30 s, 6. 72°C 3 s, 7. Plate reading, and 8. go to step 3 for 50 additional cycles; *Cdc25a* 3′ end: 1. 50°C 30 min, 2. 95°C 15 min, 3. 94°C 15 s, 4. 57°C 30 s, 5. 72°C 30 s, 6. 72°C 3 s, 7. plate reading, and 8. go to step 3 for 50 additional cycles; *Gfp*: 1. 50°C 30 min, 2. 95°C 15 min, 3. 94°C 15 s, 4. 50°C 30 s, 5. 72°C 30 s, 6. 72°C 3 s, 7. plate reading, and 8. go to step 3 for 50 additional cycles. Following quantification of the PCR reaction product, expected size of product was verified by electrophoresis using 1% agarose gel. The product sizes were the following: *Cdc25a* 5′ end—99 bp, *Cdc25a* 3′ end—124 bp, and *Gfp*—122 bp. Raw data without smoothening and with a global minimum baseline correction were imported into Excel; initial amount of mRNA was calculated and *Cdc25a* mRNA expression was normalized to *Gfp* mRNA. Graphs represent relative *Cdc25a* mRNA expression in relative arbitrary units.

Immunoblotting

Sperm from ICR (CD-1) males were prepared as in Fenclová *et al* (2022) and were a gift from Jan Nevoral, Charles University, Pilsen, Czech Republic. For immunoblotting, sample amount, collecting time, and stage are indicated in the appropriate Figure Legends. Embryos were checked for any remaining cumulus cells and 3× washed in PBS supplied with 1 mg/ml poly(vinyl alcohol) and only embryos without PBS were frozen at −80°C.

Before immunoblotting, the embryos were lysed in 10–20 μl 1× NuPAGE™ LDS Sample Buffer (Thermo Fisher Scientific, NP0007) supplied with 1× Invitrogen™ NuPAGE™ Sample Reducing Agent (Thermo Fisher Scientific, NP0004) and 1× Halt™ Protease and Phosphatase Inhibitor Cocktail (Thermo Fisher Scientific, 1861281) or Phosphatase Inhibitor Cocktail Set III (Merck, 524627-1ML). The samples were lysed at 100°C for 4 min. Electrophoresis was conducted at 150 V for 4 h on ice in NuPAGE™ MES SDS Running Buffer (20×; Thermo Fisher Scientific, NP0002) supplied with 1× NuPAGE™ Antioxidant (Thermo Fisher Scientific, NP0005) using NUPAGE 4–12% BT GEL 1.5MM 10 W (Thermo Fisher Scientific, NP0335BOX) and Page Ruler PLUS prestained protein ladder (Thermo Fisher Scientific, 26619). The proteins were blotted using a dry blotting system Trans-Blot Turbo Transfer System (Bio-Rad, 1704150) with Trans-Blot Turbo RTA Mini Nitrocellulose Transfer Kit (Biorad, 1704270). A loading control was performed by total protein staining using Pierce Reversible Protein Stain Kit for

Nitrocellulose Membranes (Thermo Fisher Scientific, 24580). For blocking, the membrane was washed in 5% milk in 0.05% Tris-buffer saline-Tween (TBST), pH 7.4 for 1 h. The membrane was then incubated in 1:500 CHK1 (G-4) Antibody (Santa Cruz Biotechnology, sc8408) diluted in 5% milk at 4°C overnight. After 3× washing in TBST for 10 min, the membranes were incubated for 1 h in Peroxidase AffiniPure Donkey Anti-Mouse IgG (Jackson Immuno Research, 715-035-151) diluted 1:5,000 in 5% milk in TBST. The membranes were washed 3× in TBST for 10 min again and afterward incubated in Immobilon ECL Ultra Western HRP Substrate (Merck, WBULS0100) for 2–5 min and scanned with GS-800 densitometer (Bio-Rad).

Immunofluorescence

Immunofluorescence was performed as described in Ruth *et al* (2021). For quantitative DAPI signal measurements, *Chk1* WT and *Chk1* mKO two-cell stage embryos were initially incubated in 60 μg/ml RNase A Solution (Dynex, #158922) before DAPI staining in a single experiment without EdU and γH2AX staining. We found that the initial RNase treatment was not required and therefore was omitted. Embryos were mounted in ProLong Gold Antifade Mountant with DAPI (Invitrogen, P36941) or laboratory-made Mowiol with 0.25 μg/ml DAPI for DNA staining (Mayer *et al*, 2016).

For EdU pulse staining, embryos were initially incubated with 100 μM EdU (5-ethynyl-2′-deoxyuridine; Merck, T511285) for 1 h before washing and fixation. After the permeabilization step, the embryos were incubated in dark at room temperature for 2 h in freshly prepared 10 μM AlexaFluor 488 azide (Invitrogen, A10266) in PBS supplemented with 1 mM copper (II) sulfate ($CuSO_4$; Merck, C1297) and 10 mM sodium-L-ascorbate (Merck, 11140).

Confocal microscopy

Samples were scanned using a confocal microscope Leica TCS SP5 with HCX PlApo Lambda Blue 63× 1.4 oil objective. We applied a sequential scan with 400 Hz, 12-bit depth, 512 × 512 pixels with 120 nm pixel size, zoom 4, line average 3, and 1 μm z-sections. TRITC was excited by 561 laser, EdU by 488 laser, and DAPI by 405 laser. TRITC and Alexa were scanned using HyD detectors, and DAPI was scanned using PMT detector.

Time-lapse imaging

Bright-field time-lapse imaging was performed on an inverted microscope Leica DMI 6000B (Leica Microsystems, Germany) in a controlled environment (37°C, 5% CO_2 in air; del Llano *et al*, 2022). Oocytes/embryos were placed in a 10 μl drop of culture medium covered with oil (oocytes: Mineral oil, Merck, M5310; embryos: OVOIL™, Vitrolife, 10029). Bright-field images were taken in 30 min intervals. Only embryos with two pronuclei that were divided into two-cell stage were included in the analysis.

Bright-field (Appendix Fig S3) and fluorescent long-term time-lapse imaging of embryos was performed on a Viventis LS1 Live light-sheet microscope (Viventis Microscopy Sarl, Switzerland), as described in Ferencova *et al* (2022). Embryos were placed in a 100 μl culture medium covered with 150 μl oil (OVOIL™, Vitrolife, 10029) in sample-holder multi-well (Viventis Microscopy, SHM1_4W). When inhibitors were used, embryos were placed in 250 μl culture medium and the dishes were covered with parafilm with small holes to allow gas exchange. Images were taken using a pixel resolution of 750 × 750 (until the eight-cell stage) or 1,024 × 1,024 (until morula/blastocyst stage) with pixel size of 173 nm, 3 μm optical sections, and 10-min time intervals. Only embryos with two pronuclei that were divided into two-cell stage were included in the analysis.

Because both two- to three- and three- to four-stage cell divisions represent second embryonic division, we chose to show two- to three-cell stage division. On the other hand, in assessing chromosome segregation errors, we scored both two- to three- and three- to four-stage cell divisions to represent the entire second embryonic division.

Image analysis

Image analysis was performed using Fiji software (Schindelin *et al*, 2012). Cell cycle phases were determined using 60 min EdU pulse staining, temporal information, and chromosome condensation state as shown by DAPI staining. EdU-positive embryos were scored as in S phase. EdU-negative embryos were classified as being in G2. Mitosis was detected by the state of chromosome condensation from DAPI staining. The number of γH2AX foci was determined by the Findfoci algorithm for Fiji (Herbert *et al*, 2014). DNA content by DAPI staining was measured as a sum of the pixel values of DAPI signal in the nucleus.

The mCDT1-EYFP, CDC25A-EGFP, and EGFP raw signal were measured on maximal intensity projections in X-axis. Values were normalized to maximum mean value at the peak or maximum values for EGFP. Cell cycle phase lengths from the mCDT1-EYFP sensor were determined as follows: G1 was assessed as the time from nuclear envelope assembly (marked by the nuclear mCDT1-EYFP signal appearance) until the peak value. Initiation of S phase was assessed as the first time point of a declining signal after the peak value. Completion of S phase was determined as the start of G2. Start of G2 was assessed as the first time point of the first three successive time points with rising values. End of G2 was assessed as the time of disappearance of mCDT1-EYFP signal during NEBD. For CDC25A-EGFP, signal disappearance before 25 h after nuclear assembly indicated NEBD.

For representative videos, the fluorescent images were denoised by Gaussian blur ($r = 1$), and for H2B-mCHERRY was applied an autocontrast macro.

Statistical analysis

Most data were obtained from at least two independent experiments and the data were pooled. Statistical analysis was performed using NCSS 11 software (NCSS, Kaysville UT, USA). The following tests were used: Student's *t*-test for normal data distribution with equal variances (unpaired), Aspin–Welch test for normal distribution with unequal variances (unpaired), Mann–Whitney *U* test for other continuous distributions, and Fisher's exact test for binomial distributions. The results were considered statistically significant with $P < 0.05$ depicted as $*P < 0.05$, $**P < 0.01$, and $***P < 0.001$.

Data availability

Bright-field and light-sheet time-lapse imaging, immunofluorescence, immunoblots, and image analysis of confocal or light-sheet live-cell microscopy are available in the BioStudies database under accession number S-BSST940 (https://www.ebi.ac.uk/biostudies/studies/S-BSST940). Other data are available from the corresponding author upon reasonable request.

Expanded View for this article is available online.

Acknowledgements
The authors dedicate this manuscript to the memory of Petr Solc, who directed the lab until his untimely death. D.D also thanks Jan Nevoral for the sperm samples, and Petr Svoboda and Jakub Cervenka for advice. D.D. was funded by grant #20-27742S from the Grant Agency of the Czech Republic. L.K. was supported by Ph.D. grant #1402217 from the Grant Agency of Charles University and Læge Sophus Carl Emil Friis og Hustru Olga Doris Friis' Legat. E.R.H. was supported by the European Research Council "ReCAP" (grant agreement 724718) and IRFD project 0134-00299B. V.B. was supported by grant VEGA 2/0072/19 from the Grant Agency of Slovakia.

Author contributions
Lucie Knoblochova: Conceptualization; data curation; formal analysis; funding acquisition; validation; investigation; visualization; methodology; writing – original draft; project administration; writing – review and editing. **Tomas Duricek:** Formal analysis; investigation; writing – review and editing. **Michaela Vaskovicova:** Resources; data curation; software; formal analysis; investigation; methodology; writing – review and editing. **Chrysoula Zorzompokou:** Investigation; writing – review and editing. **Diana Rayova:** Resources; methodology; writing – review and editing. **Ivana Ferencova:** Investigation; writing – review and editing. **Vladimir Baran:** Conceptualization; writing – review and editing. **Richard M Schultz:** Supervision; writing – review and editing. **Eva R Hoffmann:** Supervision; writing – review and editing. **David Drutovic:** Conceptualization; supervision; validation; writing – original draft; project administration; writing – review and editing.

Disclosure and competing interests statement
The authors declare that they have no conflict of interest.

References

Abe K-I, Funaya S, Tsukioka D, Kawamura M, Suzuki Y, Suzuki MG, Schultz RM, Aoki F (2018) Minor zygotic gene activation is essential for mouse preimplantation development. *Proc Natl Acad Sci U S A* 115: E6780 – E6788

Abramczuk J, Sawicki W (1975) Pronuclear synthesis of DNA in fertilized and parthenogenetically activated mouse eggs: a cytophotometric study. *Exp Cell Res* 92: 361 – 371

Adhikari D, Zheng W, Shen Y, Gorre N, Ning Y, Halet G (2012) Cdk1, but not Cdk2, is the sole Cdk that is essential and sufficient to drive resumption of meiosis in mouse oocytes. *Hum Mol Genet* 21: 2476 – 2484

Aoki F, Worrad DM, Schultz RM (1997) Regulation of transcriptional activity during the first and second cell cycles in the preimplantation mouse embryo. *Dev Biol* 181: 296 – 307

Artus J, Cohen-Tannoudji M (2008) Cell cycle regulation during early mouse embryogenesis. *Mol Cell Endocrinol* 282: 78 – 86

Barroso S, Herrera-Moyano E, Muñoz S, García-Rubio M, Gómez-González B, Aguilera A (2019) The DNA damage response acts as a safeguard against harmful DNA–RNA hybrids of different origins. *EMBO Rep* 20: e47250

Blengini CS, Ibrahimian P, Vaskovicova M, Drutovic D, Solc P, Schindler K (2021) Aurora kinase A is essential for meiosis in mouse oocytes. *PLoS Genet* 17: 1 – 27

Blythe SA, Wieschaus EF (2015) Zygotic genome activation triggers the DNA replication checkpoint at the midblastula transition. *Cell* 160: 1169 – 1181

Bolton VN, Oades PJ, Johnson MH (1984) The relationship between cleavage, DNA replication, and gene expression in the mouse 2-cell embryo. *J Embryol Exp Morphol* 79: 139 – 163

Bolton H, Graham SJL, Van Der Aa N, Kumar P, Theunis K, Fernandez Gallardo E, Voet T, Zernicka-Goetz M (2016) Mouse model of chromosome mosaicism reveals lineage-specific depletion of aneuploid cells and normal developmental potential. *Nat Commun* 7: 11165

Branigan TB, Kozono D, Schade AE, Deraska P, Rivas HG, Sambel L, Reavis HD, Shapiro GI, D'Andrea AD, DeCaprio JA (2021) MMB-FOXM1-driven premature mitosis is required for CHK1 inhibitor sensitivity. *Cell Rep* 34: 108808

Braude BPR (1979) Time-dependent effects of a-amanitin on blastocyst formation in the mouse. *J Embryol Exp Morphol* 52: 193 – 202

Brown EJ, Baltimore D (2000) ATR disruption leads to chromosomal fragmentation and early embryonic lethality. *Genes Dev* 14: 397 – 402

Capalbo A, Poli M, Rienzi L, Girardi L, Patassini C, Fabiani M, Cimadomo D, Benini F, Farcomeni A, Cuzzi J *et al* (2021) Mosaic human preimplantation embryos and their developmental potential in a prospective, non-selection clinical trial. *Am J Hum Genet* 108: 2238 – 2247

Carson SA, Kallen AN (2021) Diagnosis and management of infertility: a review. *JAMA* 326: 65 – 76

Cavazza T, Takeda Y, Politi AZ, Aushev M, Aldag P, Baker C, Choudhary M, Bucevičius J, Lukinavičius G, Elder K *et al* (2021) Parental genome unification is highly error-prone in mammalian embryos. *Cell* 184: 2860 – 2877

Chen M-S, Hurov J, White LS, Piwnica-worms H, Woodford-thomas T (2001) Absence of apparent phenotype in mice lacking Cdc25C protein phosphatase. *Mol Cell Biol* 21: 3853 – 3861

Chen M-S, Ryan CE, Piwnica-Worms H (2003) Chk1 kinase negatively regulates mitotic function of Cdc25A phosphatase through 14-3-3 binding. *Mol Cell Biol* 23: 7488 – 7497

Chen B, Guo J, Wang T, Lee Q, Ming J, Ding F, Li H, Zhang Z, Li L, Cao Y *et al* (2022) Maternal heterozygous mutation in CHEK1 leads to mitotic arrest in human zygotes. *Protein Cell* 13: 148 – 154

Collart C, Allen GE, Bradshaw CR, Smith JC, Zegerman P (2013) Titration of four replication factors is essential for the *Xenopus laevis* midblastula transition. *Science* 341: 893 – 896

Collart C, Smith JC, Zegerman P (2017) Chk1 inhibition of the replication factor Drf1 guarantees cell-cycle elongation at the *Xenopus laevis* mid-blastula transition. *Dev Cell* 42: 82 – 96

Currie CE, Ford E, Benham Whyte L, Taylor DM, Mihalas BP, Erent M, Marston AL, Hartshorne GM, McAinsh AD (2022) The first mitotic division of human embryos is highly error prone. *Nat Commun* 13: 6755

Dalle Nogare DE, Pauerstein PT, Lane ME (2009) G2 acquisition by transcription-independent mechanism at the zebrafish midblastula transition. *Dev Biol* 326: 131 – 142

Dandoulaki M, Petsalaki E, Sumpton D, Zanivan S, Zachos G (2018) Src activation by Chk1 promotes actin patch formation and prevents chromatin bridge breakage in cytokinesis. *J Cell Biol* 217: 3071 – 3089

Deneke VE, Melbinger A, Vergassola M, Di Talia S (2016) Waves of Cdk1 activity in S phase synchronize the cell cycle in *Drosophila* embryos. *Dev Cell* 38: 399 – 412

Domon M (1980) Cell cycle-dependent radiosensitivity in two-cell mouse embryos in culture. *Radiat Res* 81: 236 – 245

Durkin SG, Arlt MF, Howlett NG, Glover TW (2006) Depletion of CHK1, but not CHK2, induces chromosomal instability and breaks at common fragile sites. *Oncogene* 25: 4381 – 4388

Eckersley-Maslin MA, Alda-Catalinas C, Reik W (2018) Dynamics of the epigenetic landscape during the maternal-to-zygotic transition. *Nat Rev Mol Cell Biol* 19: 436 – 450

Enoch T, Nurse P (1990) Mutation of fission yeast cell cycle control genes abolishes dependence of mitosis on DNA replication. *Cell* 60: 665 – 673

Eykelenboom JK, Harte EC, Canavan L, Pastor-Peidro A, Calvo-Asensio I, Llorens-Agost M, Lowndes NF (2013) ATR activates the S-M checkpoint during unperturbed growth to ensure sufficient replication prior to mitotic onset. *Cell Rep* 5: 1095 – 1107

Fenclová T, Řimnáčová H, Chemek M, Havránková J, Klein P, Králíčková M, Nevoral J (2022) Nursing exposure to bisphenols as a cause of male idiopathic infertility. *Front Physiol* 13: 725442

Ferencova I, Vaskovicova M, Drutovic D, Knoblochova L, Macurek L, Schultz RM, Solc P (2022) CDC25B is required for the metaphase I-metaphase II transition in mouse oocytes. *J Cell Sci* 135: jcs252924

Ferguson AM, White LS, Donovan PJ, Piwnica-worms H (2005) Normal cell cycle and checkpoint responses in mice and cells lacking Cdc25B and Cdc25C protein phosphatases. *Mol Cell Biol* 25: 2853 – 2860

Fishler T, Li YY, Wang RH, Kim HS, Sengupta K, Vassilopoulos A, Lahusen T, Xu X, Lee MH, Liu Q *et al* (2010) Genetic instability and mammary tumor formation in mice carrying mammary-specific disruption of Chk1 and p53. *Oncogene* 29: 4007 – 4017

Flach G, Johnson MH, Braude PR, Ra T, Bolton VN (1982) The transition from maternal to embryonic control in the 2-cell mouse embryo. *EMBO J* 1: 681 – 686

Foe VE, Alberts BM (1983) Studies of nuclear and cytoplasmic behaviour during the five mitotic cycles that precede gastrulation in *Drosophila* embryogenesis. *J Cell Sci* 61: 31 – 70

Galaktionov K, Beach D (1991) Specific activation of cdc25 tyrosine phosphatases by B-type cyclins: evidence for multiple roles of mitotic cyclins. *Cell* 67: 1181 – 1194

González Besteiro MA, Gottifredi V (2015) The fork and the kinase: a DNA replication tale from a CHK1 perspective. *Mutat Res Rev Mutat Res* 763: 168 – 180

Goto H, Natsume T, Kanemaki MT, Kaito A, Wang S, Gabazza EC, Inagaki M, Mizoguchi A (2019) Chk1-mediated Cdc25A degradation as a critical mechanism for normal cell cycle progression. *J Cell Sci* 132: jcs223123

Graf A, Krebs S, Zakhartchenko V, Schwalb B, Blum H, Wolf E (2014) Fine mapping of genome activation in bovine embryos by RNA sequencing. *Proc Natl Acad Sci U S A* 111: 4139 – 4144

Gruhn JR, Hoffmann ER (2022) Errors of the egg: the establishment and progression of human aneuploidy research in the maternal germline. *Annu Rev Genet* 56: 369 – 390

Hadjantonakis A-K, Papaioannou VE (2004) Dynamic *in vivo* imaging and cell tracking using a histone fluorescent protein fusion in mice. *BMC Biotechnol* 4: 33

Hamatani T, Carter MG, Sharov AA, Ko MSH (2004) Dynamics of global gene expression changes during mouse preimplantation development. *Dev Cell* 6: 117 – 131

Hartley RS, Rempel RE, Maller JL (1996) *In vivo* regulation of the early embryonic cell cycle in Xenopus. *Dev Biol* 173: 408 – 419

Hartwell LH, Weinert TA (1989) Checkpoints: controls that ensure the order of cell cycle events. *Science* 246: 629 – 634

Herbert AD, Carr AM, Hoffmann E, Lichten M (2014) FindFoci: a focus detection algorithm with automated parameter training that closely matches human assignments, reduces human inconsistencies and increases speed of analysis. *PLoS One* 9: 1 – 33

Hoffelder DR, Luo L, Burke NA, Watkins SC, Gollin SM, Saunders WS (2004) Resolution of anaphase bridges in cancer cells. *Chromosoma* 112: 389 – 397

Holway AH, Kim S-H, La Volpe A, Michael WM (2006) Checkpoint silencing during the DNA damage response in *Caenorhabditis elegans* embryos. *J Cell Biol* 172: 999 – 1008

Hörmanseder E, Tischer T, Mayer TU (2013) Modulation of cell cycle control during oocyte-to-embryo transitions. *EMBO J* 32: 2191 – 2203

Howlett SK, Bolton VN (1985) Sequence and regulation of morphological and molecular events during the first cell cycle of mouse embryogenesis. *Development* 87: 175 – 206

Jang W-I, Lin Z-L, Lee SH, Namgoong S, Kim N-H (2014) A specific inhibitor of CDK1, RO-3306, reversibly arrests meiosis during in vitro maturation of porcine oocytes. *Anim Reprod Sci* 144: 102 – 108

Ju JQ, Li XH, Pan MH, Xu Y, Sun MH, Xu Y, Sun SC (2020) CHK1 monitors spindle assembly checkpoint and DNA damage repair during the first cleavage of mouse early embryos. *Cell Prolif* 53: e12895

Kalogeropoulos N, Christoforou C, Green AJ, Gill S, Ashcroft NR (2004) chk-1 is an essential gene and is required for an S-M checkpoint during early embryogenesis. *Cell Cycle* 3: 1196 – 1200

Kitajima TS, Ohsugi M, Ellenberg J (2011) Complete kinetochore tracking reveals error-prone homologous chromosome biorientation in mammalian oocytes. *Cell* 146: 568 – 581

Knowland J, Graham C (1972) RNA synthesis at the two-cell stage of mouse development. *J Embryol Exp Morphol* 27: 167 – 176

Kobayashi H, Sakurai T, Imai M, Takahashi N, Fukuda A, Yayoi O, Sato S, Nakabayashi K, Hata K, Sotomaru Y *et al* (2012) Contribution of intragenic DNA methylation in mouse gametic DNA methylomes to establish oocyte-specific heritable marks. *PLoS Genet* 8: e1002440

Kramer A, Mailand N, Lukas C, Syljuasen RG, Wilkinson CJ, Nigg EA, Bartek J, Lukas J (2004) Centrosome-associated Chk1 prevents premature activation of cyclin-B-Cdk1 kinase. *Nat Cell Biol* 6: 884 – 891

Krishna M, Generoso WM (1977) Timing of sperm penetration, pronuclear formation, pronuclear DNA synthesis, and first cleavage in naturally ovulated mouse eggs. *J Exp Zool* 202: 245 – 252

Ladstätter S, Tachibana-Konwalski K (2016) A surveillance mechanism ensures repair of DNA lesions during zygotic reprogramming. *Cell* 167: 1774 – 1787

Lam MH, Liu Q, Elledge SJ, Rosen JM (2004) Chk1 is haploinsufficient for multiple functions critical to tumor suppression. *Cancer Cell* 6: 45 – 59

Lam FC, Kong YW, Huang Q, Vu Han T-L, Maffa AD, Kasper EM, Yaffe MB (2020) BRD4 prevents the accumulation of R-loops and protects against transcription-replication collision events and DNA damage. *Nat Commun* 11: 4083

Lebrec V, Poteau M, Morretton J-P, Gavet O (2022) Chk1 dynamics in G2 phase upon replication stress predict daughter cell outcome. *Dev Cell* 57: 638 – 653

Lee G, White LS, Hurov KE, Stappenbeck TS, Piwnica-Worms H (2009) Response of small intestinal epithelial cells to acute disruption of cell division through CDC25 deletion. *Proc Natl Acad Sci U S A* 106: 4701 – 4706

Lemmens B, Hegarat N, Akopyan K, Sala-Gaston J, Bartek J, Hochegger H, Lindqvist A (2018) DNA replication determines timing of mitosis by restricting CDK1 and PLK1 activation. *Mol Cell* 71: 117 – 128

Lewandoski M, Wassarman KM, Martin GR (1997) Zp3–cre, a transgenic mouse line for the activation or inactivation of loxP-flanked target genes specifically in the female germ line. *Curr Biol* 7: 148 – 151

Li Y, Sun J, Ling Y, Ming H, Chen Z, Fang F, Liu Y, Cao H, Ding J, Cao Z *et al* (2020) Transcription profiles of oocytes during maturation and embryos during preimplantation development in vivo in the goat. *Reprod Fertil Dev* 32: 714 – 725

Lincoln AJ, Wickramasinghe D, Stein P, Schultz RM, Palko ME, De Miguel MP, Tessarollo L, Donovan PJ (2002) Cdc25b phosphatase is required for resumption of meiosis during oocyte maturation. *Nat Genet* 30: 446 – 449

Liu Q, Guntuku S, Cui XS, Matsuoka S, Cortez D, Tamai K, Luo G, Carattini-Rivera S, DeMayo F, Bradley A *et al* (2000) Chk1 is an essential kinase that is regulated by Atr and required for the G2/M DNA damage checkpoint. *Genes Dev* 14: 1448 – 1459

del Llano E, Iyyappan R, Aleshkina D, Masek T, Dvoran M, Jiang Z, Pospisek M, Kubelka M, Susor A (2022) SGK1 is essential for meiotic resumption in mammalian oocytes. *Eur J Cell Biol* 101: 151210

Löffler H, Rebacz B, Ho AD, Lukas J, Bartek J, Krämer A (2006) Chk1-dependent regulation of Cdc25B functions to coordinate mitotic events. *Cell Cycle* 5: 2543 – 2547

Mah LJ, El-Osta A, Karagiannis TC (2010) γH2AX: a sensitive molecular marker of DNA damage and repair. *Leukemia* 24: 679 – 686

Mailand N, Falck J, Lukas C, Syljuâsen RG, Welcker M, Bartek J, Lukas J (2000) Rapid destruction of human Cdc25A in response to DNA damage. *Science* 288: 1425 – 1429

Mailand N, Podtelejnikov VA, Groth A, Mann M, Bartek J, Lukas J (2002) Regulation of G(2)/M events by Cdc25A through phosphorylation-dependent modulation of its stability. *EMBO J* 21: 5911 – 5920

Mashiko D, Ikeda Z, Yao T, Tokoro M, Fukunaga N, Asada Y, Yamagata K (2020) Chromosome segregation error during early cleavage in mouse pre-implantation embryo does not necessarily cause developmental failure after blastocyst stage. *Sci Rep* 10: 1 – 10

Mayer A, Baran V, Sakakibara Y, Brzakova A, Ferencova I, Motlik J, Kitajima TS, Schultz RM, Solc P (2016) DNA damage response during mouse oocyte maturation. *Cell Cycle* 15: 546 – 558

McCoy RC, Summers MC, McCollin A, Ottolini CS, Ahuja K, Handyside AH (2022) Meiotic and mitotic aneuploidies drive arrest of *in vitro* fertilized human preimplantation embryos. *bioRxiv* https://doi.org/10.1101/2022.07.03.498614 [PREPRINT]

Michelena J, Gatti M, Teloni F, Imhof R, Altmeyer M (2019) Basal CHK1 activity safeguards its stability to maintain intrinsic S-phase checkpoint functions. *J Cell Biol* 218: 2865 – 2875

Mocanu C, Karanika E, Fernandez-Casanas M, Herbert A, Olukoga T, Ozgurses ME, Chan KL (2022) DNA replication is highly resilient and persistent under the challenge of mild replication stress. *Cell Rep* 39: 110701

Moiseeva TN, Yin Y, Calderon MJ, Qian C, Schamus-haynes S, Sugitani N (2019) An ATR and CHK1 kinase signaling mechanism that limits origin firing during unperturbed DNA replication. *Proc Natl Acad Sci U S A* 116: 13374 – 13383

Molinari M, Mercurio C, Dominguez J, Goubin F, Draetta GF (2000) Human Cdc25 A inactivation in response to S phase inhibition and its role in preventing premature mitosis. *EMBO Rep* 1: 71 – 79

Molls M, Zamboglou N, Streffer C (1983) A comparison of the cell kinetics of pre-implantation mouse embryos from two different mouse strains. *Cell Tissue Kinet* 16: 277 – 283

Muralidharan VS, Nilsson LM, Lindberg MF, Nilsson JA (2020) Small molecule inhibitors and a kinase-dead expressing mouse model demonstrate that the kinase activity of Chk1 is essential for mouse embryos and cancer cells. *Life Sci Alliance* 3: 1 – 9

Nagata A, Igarashi M, Jinno S, Suto K, Okayama H (1991) An additional homolog of the fission yeast cdc25^{+} gene occurs in humans and is highly expressed in some cancer cells. *New Biol* 3: 959 – 968

Newport J, Kirschner M (1982) A major developmental transition in early xenopus embryos: I. characterization and timing of cellular changes at the midblastula stage. *Cell* 30: 675 – 686

Niida H, Tsuge S, Katsuno Y, Konishi A, Takeda N, Nakanishi M (2005) Depletion of Chk1 leads to premature activation of Cdc2-cyclin B and mitotic catastrophe. *J Biol Chem* 280: 39246 – 39252

Nothias J-Y, Majumder S, Kaneko KJ, DePamphilis ML (1995) Regulation of gene expression at the beginning of mammalian development. *J Biol Chem* 270: 22077 – 22080

Palmer N, Kaldis P (2016) Chapter One – Regulation of the embryonic cell cycle during mammalian preimplantation development. In *Mammalian Preimplantation Development*, DePamphilis ML (ed), pp 1 – 53. Cambridge, MA: Academic Press

Palmerola KL, Amrane S, Angeles ADL, Koren A, Baslan T, Egli D, Palmerola KL, Amrane S, Angeles ADL, Xu S *et al* (2022) Replication stress impairs chromosome segregation and preimplantation development in human embryos. *Cell* 185: 2988 – 3007

Park S-J, Komata M, Inoue F, Yamada K, Nakai K, Ohsugi M, Shirahige K (2013) Inferring the choreography of parental genomes during fertilization from ultralarge-scale whole-transcriptome analysis. *Genes Dev* 27: 2736 – 2748

Peddibhotla S, Lam MH, Gonzalez-Rimbau M, Rosen JM (2009) The DNA-damage effector checkpoint kinase 1 is essential for chromosome segregation and cytokinesis. *Proc Natl Acad Sci U S A* 106: 5159 – 5164

Peng CY, Graves PR, Thoma RS, Wu Z, Shaw AS, Piwnica-Worms H (1997) Mitotic and G2 checkpoint control: regulation of 14-3-3 protein binding by phosphorylation of Cdc25C on serine-216. *Science* 277: 1501 – 1505

Petrus MJ, Wilhelm DE, Murakami M, Kappas NC, Carter AD, Wroble BN, Sible JC (2004) Altered expression of Chk1 disrupts cell cycle remodeling at the midblastula transition in *Xenopus laevis* embryos. *Cell Cycle* 3: 212 – 217

Pomerening JR, Sontag ED, Ferrell JE Jr (2003) Building a cell cycle oscillator: hysteresis and bistability in the activation of Cdc2. *Nat Cell Biol* 5: 346 – 351

Qiu JJ, Zhang WW, Wu ZL, Wang YH, Qian M, Li YP (2003) Delay of ZGA initiation occurred in 2-cell blocked mouse embryos. *Cell Res* 13: 179 – 185

Radonova L, Svobodova T, Anger M (2019) Regulation of the cell cycle in early mammalian embryos and its clinical implications. *Int J Dev Biol* 63: 113 – 122

Rambhatla L, Latham KE (1995) Strain-specific progression of α-amanitin—treated mouse embryos beyond the two-cell stage. *Mol Reprod Dev* 41: 16 – 19

Ray D, Terao Y, Nimbalkar D, Hirai H, Osmundson EC, Zou X, Franks R, Christov K, Kiyokawa H (2007) Hemizygous disruption of Cdc25A inhibits cellular transformation and mammary tumorigenesis in mice. *Cancer Res* 67: 6605 – 6612

Ruth KS, Day FR, Hussain J, Martínez-Marchal A, Aiken CE, Azad A, Thompson DJ, Knoblochova L, Abe H, Tarry-Adkins JL *et al* (2021) Genetic insights into biological mechanisms governing human ovarian ageing. *Nature* 596: 393 – 397

Sadhu K, Reed SI, Richardson H, Russell P (1990) Human homolog of fission yeast cdc25 mitotic inducer is predominantly expressed in G2. *Proc Natl Acad Sci U S A* 87: 5139 – 5143

Sakaue-Sawano A, Yo M, Komatsu N, Hiratsuka T, Kogure T, Hoshida T, Goshima N, Matsuda M, Miyoshi H, Miyawaki A (2017) Genetically encoded tools for optical dissection of the mammalian cell cycle. *Mol Cell* 68: 626 – 640

Saldivar JC, Hamperl S, Bocek MJ, Chung M, Bass TE, Cisneros-Soberanis F, Samejima K, Xie L, Paulson JR, Earnshaw WC *et al* (2018) An intrinsic S/G (2) checkpoint enforced by ATR. *Science* 361: 806 – 810

Sanchez Y, Wong C, Thoma RS, Richman R, Wu Z, Piwnica-Worms H, Elledge SJ (1997) Conservation of the Chk1 checkpoint pathway in mammals:

linkage of DNA damage to Cdk regulation through Cdc25. *Science* 277: 1497 – 1501

Sankar A, Lerdrup M, Manaf A, Johansen JV, Gonzalez JM, Borup R, Blanshard R, Klungland A, Hansen K, Andersen CY *et al* (2020) KDM4A regulates the maternal-to-zygotic transition by protecting broad H3K4me3 domains from H3K9me3 invasion in oocytes. *Nat Cell Biol* 22: 380 – 388

Santamaría D, Barrière C, Cerqueira A, Hunt S, Tardy C, Newton K, Cáceres JF, Dubus P, Malumbres M, Barbacid M (2007) Cdk1 is sufficient to drive the mammalian cell cycle. *Nature* 448: 811 – 815

Saskova A, Solc P, Baran V, Kubelka M, Schultz RM, Motlik J (2008) Aurora kinase a controls meiosis I progression in mouse oocytes. *Cell Cycle* 7: 2368 – 2376

Schindelin J, Arganda-Carreras I, Frise E, Kaynig V, Longair M, Pietzsch T, Preibisch S, Rueden C, Saalfeld S, Schmid B *et al* (2012) Fiji: an open-source platform for biological-image analysis. *Nat Methods* 9: 676 – 682

Schmitt E, Boutros R, Froment C, Monsarrat B, Ducommun B, Dozier C (2006) CHK1 phosphorylates CDC25B during the cell cycle in the absence of DNA damage. *J Cell Sci* 119: 4269 – 4275

Sedelnikova OA, Rogakou EP, Panyutin IG, Bonner WM (2002) Quantitative detection of (125)IdU-induced DNA double-strand breaks with gamma-H2AX antibody. *Radiat Res* 158: 486 – 492

Sha W, Moore J, Chen K, Lassaletta AD, Yi C-S, Tyson JJ, Sible JC (2003) Hysteresis drives cell-cycle transitions in *Xenopus laevis* egg extracts. *Proc Natl Acad Sci U S A* 100: 975 – 980

Shimuta K, Nakajo N, Uto K, Hayano Y, Okazaki K, Sagata N (2002) Chk1 is activated transiently and targets Cdc25A for degradation at the *Xenopus* midblastula transition. *EMBO J* 21: 3694 – 3703

Sibon OCM, Stevenson VA, Theurkauf WE (1997) DNA-replication checkpoint control at the *Drosophila* midblastula transition. *Nature* 388: 93 – 97

Solc P, Saskova A, Baran V, Kubelka M, Schultz RM, Motlik J (2008) CDC25A phosphatase controls meiosis I progression in mouse oocytes. *Dev Biol* 317: 260 – 269

Solc P, Kitajima TS, Yoshida S, Brzakova A, Kaido M, Baran V, Mayer A, Samalova P, Motlik J, Ellenberg J (2015) Multiple requirements of PLK1 during mouse oocyte maturation. *PLoS One* 10: e0116783

Sollier J, Cimprich KA (2015) Breaking bad: R-loops and genome integrity. *Trends Cell Biol* 25: 514 – 522

Sorensen CS, Syljuasen RG, Falck J, Schroeder T, Ronnstrand L, Khanna KK, Zhou B-B, Bartek J, Lukas J (2003) Chk1 regulates the S phase checkpoint by coupling the physiological turnover and ionizing radiation-induced accelerated proteolysis of Cdc25A. *Cancer Cell* 3: 247 – 258

Spencer SL, Cappell SD, Tsai FC, Overton KW, Wang CL, Meyer T (2013) The proliferation-quiescence decision is controlled by a bifurcation in CDK2 activity at mitotic exit. *Cell* 155: 369 – 383

Suski JM, Ratnayeke N, Braun M, Zhang T, Strmiska V, Michowski W, Can G, Simoneau A, Snioch K, Cup M *et al* (2022) CDC7-independent G1/S transition revealed by targeted protein degradation. *Nature* 605: 357 – 365

Svoboda P (2018) Mammalian zygotic genome activation. *Semin Cell Dev Biol* 84: 118 – 126

Syljuåsen RG, Sørensen CS, Hansen LT, Fugger K, Lundin C, Johansson F, Helleday T, Sehested M, Lukas J, Bartek J (2005) Inhibition of human Chk1 causes increased initiation of DNA replication, phosphorylation of ATR targets, and DNA breakage. *Mol Cell Biol* 25: 3553 – 3562

Takai H, Tominaga K, Motoyama N, Minamishima YA, Nagahama H, Tsukiyama T, Ikeda K, Nakayama K, Nakanishi M, Nakayama KI (2000) Aberrant cell cycle checkpoint function and early embryonic death in Chk1(–/–) mice. *Genes Dev* 14: 1439 – 1447

Tsai TY, Theriot JA, Ferrell JE Jr (2014) Changes in oscillatory dynamics in the cell cycle of early *Xenopus laevis* embryos. *PLoS Biol* 12: e1001788

Tse AN, Rendahl KG, Sheikh T, Cheema H, Aardalen K, Embry M, Ma S, Moler EJ, Ni ZJ, Lopes de Menezes DE *et al* (2007) CHIR-124, a novel potent inhibitor of Chk1, potentiates the cytotoxicity of topoisomerase I poisons *in vitro* and *in vivo*. *Clin Cancer Res* 13: 591 – 602

Vanneste E, Voet T, Melotte C, Debrock S, Sermon K, Staessen C, Liebaers I, Fryns J-P, D'Hooghe T, Vermeesch JR (2009) What next for preimplantation genetic screening? High mitotic chromosome instability rate provides the biological basis for the low success rate. *Hum Reprod* 24: 2679 – 2682

Vassilev LT, Tovar C, Chen S, Knezevic D, Zhao X, Sun H, Heimbrook DC, Chen L (2006) Selective small-molecule inhibitor reveals critical mitotic functions of human CDK1. *Proc Natl Acad Sci U S A* 103: 10660 – 10665

Xie D, Chen CC, Ptaszek LM, Xiao S, Cao X, Fang F, Ng HH, Lewin HA, Cowan C, Zhong S (2010) Rewirable gene regulatory networks in the preimplantation embryonic development of three mammalian species. *Genome Res* 20: 804 – 815

Xu Q, Wang F, Xiang Y, Zhang X, Zhao Z-A, Gao Z, Liu W, Lu X, Liu Y, Yu X-J *et al* (2015) Maternal BCAS2 protects genomic integrity in mouse early embryonic development. *Development* 142: 3943 – 3953

Xue Z, Huang K, Cai C, Cai L, Jiang C-y, Feng Y, Liu Z, Zeng Q, Cheng L, Sun YE *et al* (2013) Genetic programs in human and mouse early embryos revealed by single-cell RNA sequencing. *Nature* 500: 593 – 597

Zachos G, Rainey MD, Gillespie DAF (2003) Chk1-deficient tumour cells are viable but exhibit multiple checkpoint and survival defects. *EMBO J* 22: 713 – 723

Zachos G, Rainey MD, Gillespie DAF (2005) Chk1-dependent S-M checkpoint delay in vertebrate cells is linked to maintenance of viable replication structures. *Mol Cell Biol* 25: 563 – 574

Zachos G, Black EJ, Walker M, Scott MT, Vagnarelli P, Earnshaw WC, Gillespie DAF (2007) Chk1 is required for spindle checkpoint function. *Dev Cell* 12: 247 – 260

Zamir E, Kam Z, Yarden A (1997) Transcription-dependent induction of G1 phase during the zebra fish midblastula transition. *Mol Cell Biol* 17: 529 – 536

Zeng F, Schultz RM (2005) RNA transcript profiling during zygotic gene activation in the preimplantation mouse embryo. *Dev Biol* 283: 40 – 57

Zeng F, Baldwin DA, Schultz RM (2004) Transcript profiling during preimplantation mouse development. *Dev Biol* 272: 483 – 496

Zhang M, Kothari P, Mullins M, Lampson MA (2014) Regulation of zygotic genome activation and DNA damage checkpoint acquisition at the mid-blastula transition. *Cell Cycle* 13: 3828 – 3838

Zhang H, Chen T, Wu K, Hou Z, Zhao S, Zhang C, Gao Y, Gao M, Chen ZJ, Zhao H (2021) Dominant mutations in CHK1 cause pronuclear fusion failure and zygote arrest that can be rescued by CHK1 inhibitor. *Cell Res* 31: 814 – 817

Zhao H, Watkins JL, Piwnica-worms H (2002) Disruption of the checkpoint kinase 1/cell division cycle 25A pathway abrogates ionizing radiation-induced S and G 2 checkpoints. *Proc Natl Acad Sci U S A* 99: 14795 – 14800

Zonderland G, Vanzo R, Gadi SA, Martín-Doncel E, Coscia F, Mund A, Lerdrup M, Benada J, Boos D, Toledo L (2022) The TRESLIN-MTBP complex couples completion of DNA replication with S/G2 transition. *Mol Cell* 82: 3350 – 3365

Expanded View Figures

Figure EV1. Maternally expressed CHK1 regulates early embryonic development.

A Schematic depiction of Cre-recombinase expression specifically in growing oocytes under *zona pellucida 3 (Zp3)* promoter.

B Schematic depiction of *Chk1* gene with indicated protein domains. Exon 2 of *Chk1*, which contains a translation initiation site and is flanked by LoxP sites, is excised by Cre-recombinase, thereby preventing translation initiation of full-length *Chk1* mRNA.

C Female mice carrying floxed *Chk1* exon 2 and Cre-recombinase under oocyte-specific *Zp3* promoter are mated with *Chk1* wild-type (WT) male producing maternal *Chk1* knock-out embryos with present paternal allele (*Chk1 mKO*).

D CHK1 protein level detected by immunoblot from positive controls (10 germinal vesicle (GV) stage oocytes microinjected with full-length 300 ng/μl of *Chk1* cRNA), 10 GV oocytes (GV WT), and sperm (0.22×10^6). kDa—kilodalton.

E CHK1 protein levels detected by immunoblot in *Chk1* WT and *Chk1* mKO zygotes at 26 h post-hCG administration.

F Proportion of zygotes developed to blastocysts after pharmacological CHK1 inhibition in C57J/BL6 or CD-1 females. The numbers in brackets denote the number of analyzed embryos. Error bars denote the 95% confidence interval. ***$P = 0.00000$ (Fisher's exact test, two-sided).

G Data from bright-field time-lapse imaging (Fig 1B) were used to quantify the division time (h) from zygote to two-cell in *Chk1* WT, *Chk1* mKO *class I*, and *Chk1* mKO *class II* embryos categorized retrospectively based on their division timing to the three-cell stage, related to Fig 1B–F. The numbers in parentheses show the number of embryos analyzed for each genotype. The median is shown. ns, non-significant, $P = 0.135868$, **$P = 0.00808$, and ***$P = 0.000026$ (Mann–Whitney *U*-test).

H Time of the two-cell to three-cell division after hCG administration relative to the zygote to two-cell division, related to Fig 1B–F. *Chk1* mKO *class I* embryos show a positive correlation between the division time from zygote to two-cell and two-cell to three-cell (Pearson's correlation coefficient of 0.7932, $P < 0.0000$). *Chk1* WT embryos show a positive correlation (Pearson's correlation coefficient of 0.4214, $P = 0.0001$) but with some substantial outliers. *Chk1* mKO *class II* shows a non-significant negative correlation (Pearson's correlation coefficient −0.3080, $P = 0.0812$).

I CHK1 protein levels detected by immunoblot from two- or three- to four-cell embryos collected 47 h post-hCG administration. $n = 79$, 79, and 78 embryos for *Chk1* WT, *Chk1* mKO *class I*, and *Chk1* mKO *class II*, respectively.

J Single-cell PCR analysis of Cre-mediated DNA recombination status in individual two-cell stage *Chk1* WT, two-cell stage *Chk1* mKO *class II*, and three-cell stage *Chk1* mKO *class I* embryos. 1 kb—1 kb ladder, *Lox*—Chk1 lox/lox, PC—positive control, NC—negative control.

K Proportion of *class I* embryos indicated for individual mice. The embryos were scored at 46–47 h post-hCG administration. The numbers in brackets denote the number of mice. Data are shown as box and whisker plots, where central band represents median, upper and lower quartiles are the ends of the box, and whiskers box edges ±15%. ***$P = 0.000002$ (Mann–Whitney *U*-test).

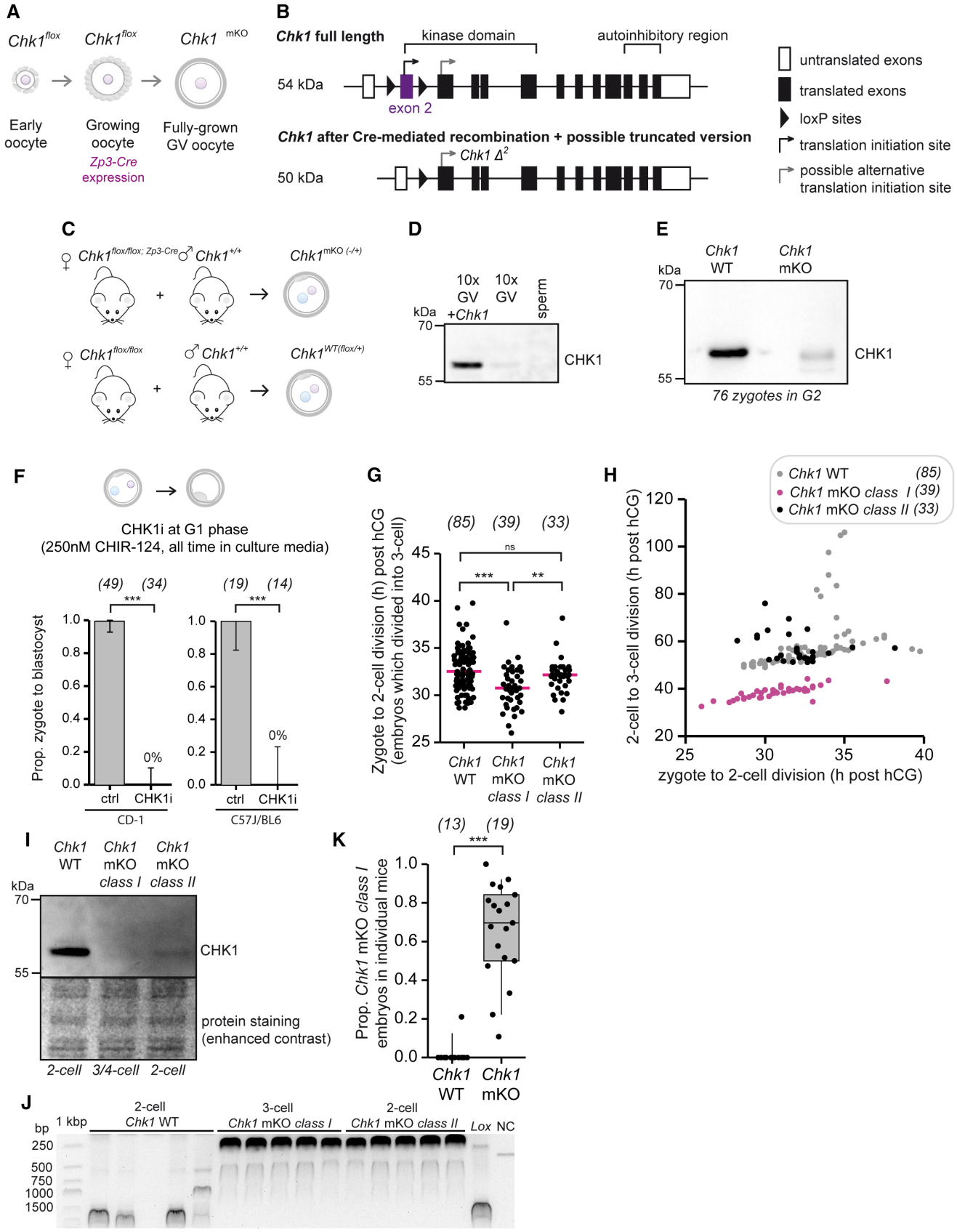

Figure EV1.

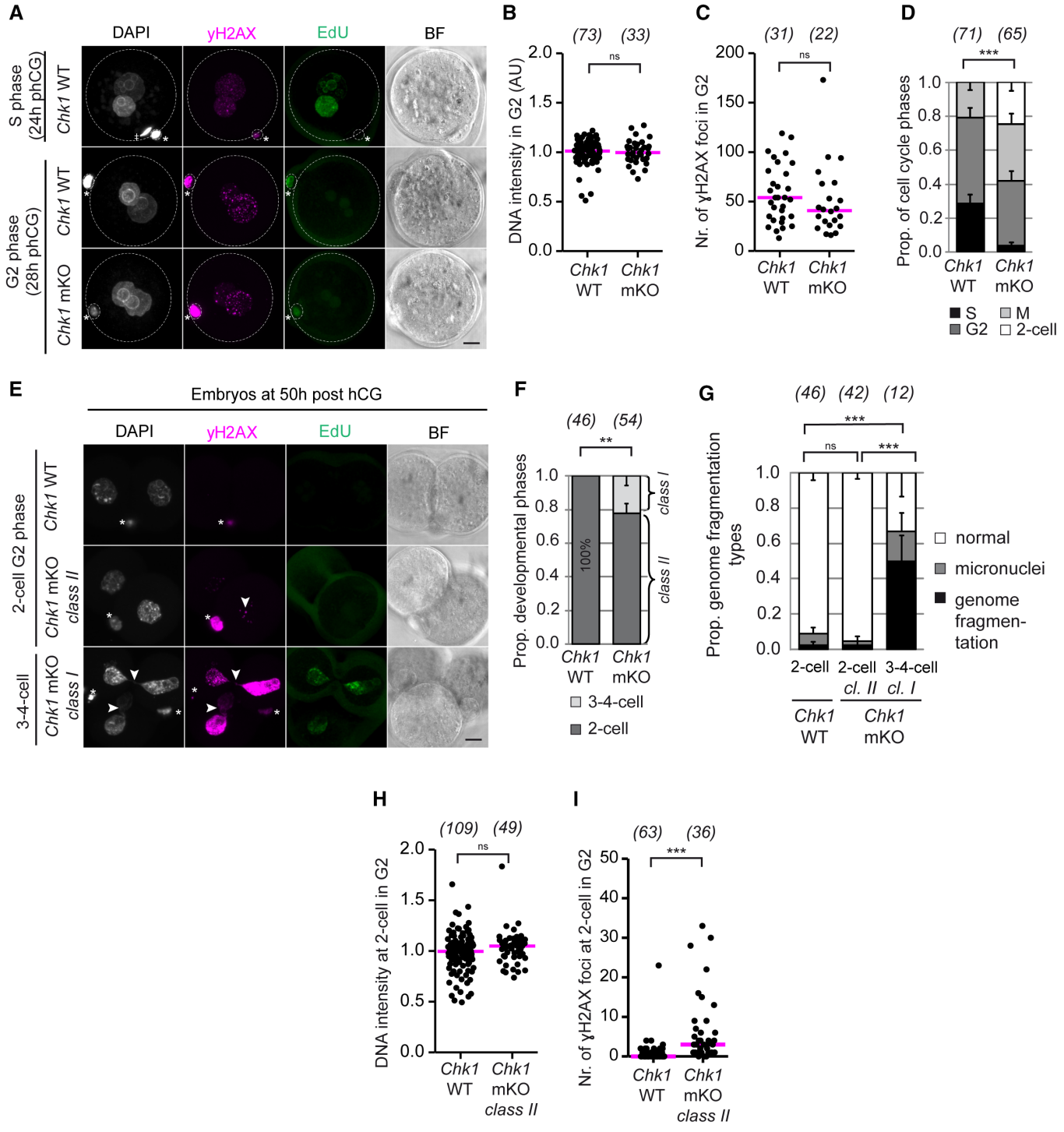
A
DAPI
γH2AX
EdU
BF
S phase (24h phCG)
Chk1 WT
G2 phase (28h phCG)
Chk1 WT
Chk1 mKO
B
(73) (33)
ns
DNA intensity in G2 (AU)
Chk1 WT
Chk1 mKO
C
(31) (22)
ns
Nr. of γH2AX foci in G2
D
(71) (65)
***
Prop. of cell cycle phases
S
G2
M
2-cell
E
Embryos at 50h post hCG
2-cell G2 phase
Chk1 mKO class II
3-4-cell
Chk1 mKO class I
F
(46) (54)
**
Prop. developmental phases
100%
class I
class II
3-4-cell
2-cell
G
(46) (42) (12)
***
ns
Prop. genome fragmentation types
normal
micronuclei
genome fragmentation
2-cell
2-cell cl. II
3-4-cell cl. I
H
(109) (49)
ns
DNA intensity at 2-cell in G2
Chk1 mKO class II
I
(63) (36)
***
Nr. of γH2AX foci at 2-cell in G2
Chk1 mKO class II

Figure EV2.

Figure EV2. CHK1 kinase regulates cell cycle progression.

A Representative still images from immunofluorescence analysis of cell cycle distribution in *Chk1* WT and *Chk1* mKO embryos combined with γH2AX foci and DNA content analysis. Zygotes in the S phase (24 h post-hCG administration) and G2 phase (28 h post-hCG administration) were fixed after a 60 min EdU pulse to identify zygotes that completed DNA replication. Embryos with γH2AX signal (magenta), DAPI (chromatin, gray), EdU (green), and BF (bright field) are shown. Asterisk marks polar bodies. Crosses mark the sperm head at the membrane. Scale bar 10 μm.

B, C Data from immunofluorescence analysis (A) were used to quantify DNA content (B) and γH2AX foci number (C) in zygotes in the G2 phase. The median is shown. DNA content was measured by DAPI intensity. The data were normalized to the mean in each group. AU (arbitrary units). The data were pooled from two independent experiments. ns, non-significant, $P = 0.727857$ (B), $P = 0.190458$ (C) (Mann–Whitney *U*-test, two-sided).

D Data from immunofluorescence analysis (A) were used to quantify the proportion of cell cycle phases in embryos. Error bars denote the standard error of the mean. ***$P = 0.00000$ (Cochran–Armitage trend test, two-sided).

E Representative still images from immunofluorescence analysis of cell cycle distribution in *Chk1* WT and *Chk1* mKO embryos combined with γH2AX foci and DNA content analysis. Embryos at 50 h post-hCG administration (G2 phase) were fixed after a 60 min EdU pulse to identify zygotes that completed DNA replication. Embryos with γH2AX signal (magenta), DAPI (chromatin, gray), EdU (green), and BF (bright field) are shown. Asterisk marks polar bodies. Arrowhead points to DNA damage visualized by γH2AX or DAPI. Scale bar 10 μm.

F, G Data from immunofluorescence analysis (E) were used to quantify the proportion of developmental phase (F) and genome fragmentation types (G) in embryos. Error bars denote the standard error of the mean. The data were pooled from two independent experiments. ns, non-significant, $P = 0.84592$, **$P = 0.00194$, ***$P = 0.00000$ (Cochran–Armitage trend test, two-sided).

H, I Data from immunofluorescence analysis (E) were used to quantify DNA content (H) and γH2AX foci number (I) in embryos at 50 h post-hCG administration. Median is shown. DNA content was measured by DAPI intensity. The data were normalized to the mean in each group. AU (arbitrary units). The data were pooled from two independent experiments. ns, non-significant, $P = 0.135607$, ***$P = 0.00000$ (Mann–Whitney *U*-test, two-sided).

Data information: The numbers in parentheses show the number of embryos analyzed for each genotype.

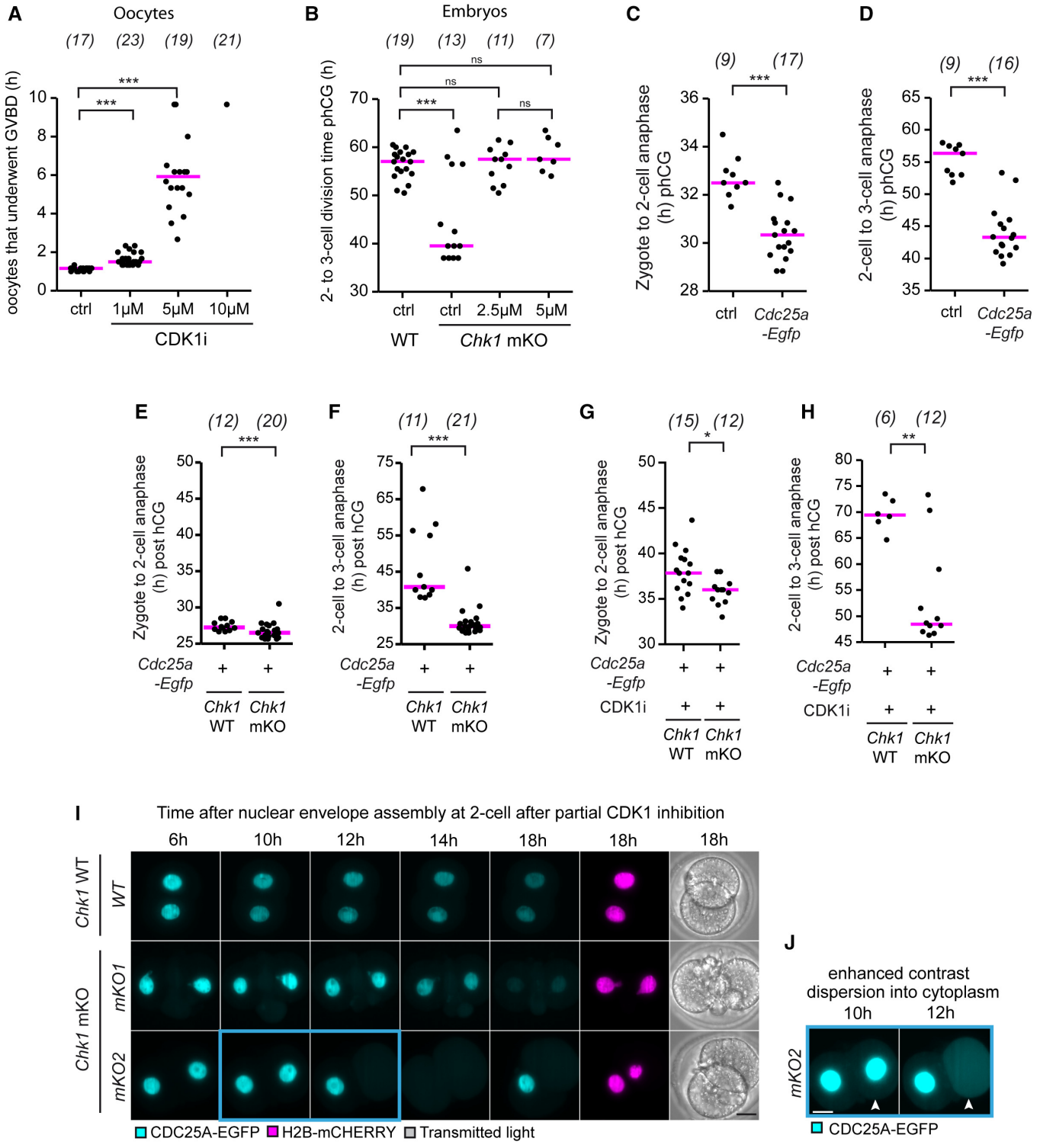
A
Oocytes
(17) (23) (19) (21)
oocytes that underwent GVBD (h)
ctrl 1μM 5μM 10μM
CDK1i
B
Embryos
(19) (13) (11) (7)
2- to 3-cell division time phCG (h)
ctrl ctrl 2.5μM 5μM
WT Chk1 mKO
C
(9) (17)
Zygote to 2-cell anaphase (h) phCG
ctrl Cdc25a -Egfp
D
(9) (16)
2-cell to 3-cell anaphase (h) phCG
ctrl Cdc25a -Egfp
E
(12) (20)
Zygote to 2-cell anaphase (h) post hCG
Cdc25a -Egfp
Chk1 WT Chk1 mKO
F
(11) (21)
2-cell to 3-cell anaphase (h) post hCG
Cdc25a -Egfp
Chk1 WT Chk1 mKO
G
(15) (12)
Zygote to 2-cell anaphase (h) post hCG
Cdc25a -Egfp
CDK1i
Chk1 WT Chk1 mKO
H
(6) (12)
2-cell to 3-cell anaphase (h) post hCG
Cdc25a -Egfp
CDK1i
Chk1 WT Chk1 mKO
I
Time after nuclear envelope assembly at 2-cell after partial CDK1 inhibition
6h 10h 12h 14h 18h 18h 18h
Chk1 WT
WT
Chk1 mKO
mKO1
mKO2
CDC25A-EGFP H2B-mCHERRY Transmitted light
J
enhanced contrast dispersion into cytoplasm
10h 12h
mKO2
CDC25A-EGFP

Figure EV3.

Figure EV3. CHK1 kinase regulates the long G2 phase in two-cell embryos by restraining CDK1 activity via CDC25A degradation.

A Dot-plot graph of GVBD time (h) analyzed from time-lapse wide-field imaging of oocytes after transfer to milrinone-free medium and treated with CDK1 kinase inhibitor (1, 5, and 10 μM RO3306). In the 10 μM RO3306 group, only 1 oocyte from 21 resumes meiosis. The data are from one experiment. ***P = 0.00000 (Mann–Whitney U-test).

B Dot-plot graph of division time (h) from two-cell to three-cell stage analyzed from time-lapse wide-field imaging of wild-type (WT) and *Chk1 mKO* embryos. The *Chk1 mKO* embryos were treated with 2.5 or 5 μM RO3306. Strain background: CD-1 with small part C57J/BL6 and C57J/BL6 with small part CD-1. ns, non-significant, ***P = 0.00034 (Kolmogorov–Smirnov test).

C, D Data from time-lapse light-sheet imaging were used to quantify the initiation of anaphase (h) from zygotes to two-cell stage embryos (C) and from two-cell to three-cell embryos (D) in WT embryos microinjected with *Cdc25a-Egfp* cRNAs. The data were pooled from two independent experiments. ***P = 0.000178 (C), P = 0.000133 (D) (Mann–Whitney U-test, two-sided).

E, F Data from time-lapse light-sheet imaging (Fig 3B) were used to quantify initiation of anaphase (h) from zygote to two-cell (E) and from two-cell to three-cell (F) in *Cdc25a*-microinjected *Chk1 WT* and *Cdc25a*-microinjected *Chk1 mKO*. Median is shown. ***P = 0.00000 (Mann–Whitney U-test, two-sided).

G, H Data from time-lapse light-sheet imaging (Fig 3E) were used to quantify initiation of first anaphase time (h) (G) and time of entry into the second mitosis (H) in *Chk1 WT* and *Chk1 mKO* embryos microinjected with *Cdc25a-Egfp* cRNA and treated with CDK1 inhibitor. Due to experimental procedures, not all embryos underwent cytokinesis after the first mitosis. Median is shown. *P = 0.015593, **P = 0.005921 (Mann–Whitney U-test, two-sided).

I Representative still images from time-lapse light-sheet imaging (Fig 3E) of *Chk1 WT* and *Chk1 mKO* embryos treated with CDK1 inhibitor. Embryos were microinjected, as shown in Fig 3E. Embryos expressing H2B-mCHERRY (magenta, chromosomes) and CDC25A-EGFP (cyan) are shown. Scale bar 20 μm. See also related Movie EV3 (*Chk1 WT* + CDC25A-EGFP + CDK1i, *Chk1 mKO (mKO1)* + CDC25A-EGFP + CDK1i, *Chk1 mKO (mKO2)* + CDC25A-EGFP + CDK1i).

J Enhanced contrast of still images of mKO2 at 10 h and 12 h. Arrowheads mark CDC25A-EGFP signal in cytoplasm. Note that cytoplasmic signals increase from 10 to 12 h, indicating that there is CDC25A-EGFP dispersed from the nucleus into cytoplasm (not degradation). Scale bar 20 μm. See also related Movie EV3 (*Chk1 WT* + CDC25A-EGFP + CDK1i, *Chk1 mKO (mKO1)* + CDC25A-EGFP + CDK1i, *Chk1 mKO (mKO2)* + CDC25A-EGFP + CDK1i).

Data information: The numbers in parentheses denote the number of analyzed oocytes per group. Median is shown.

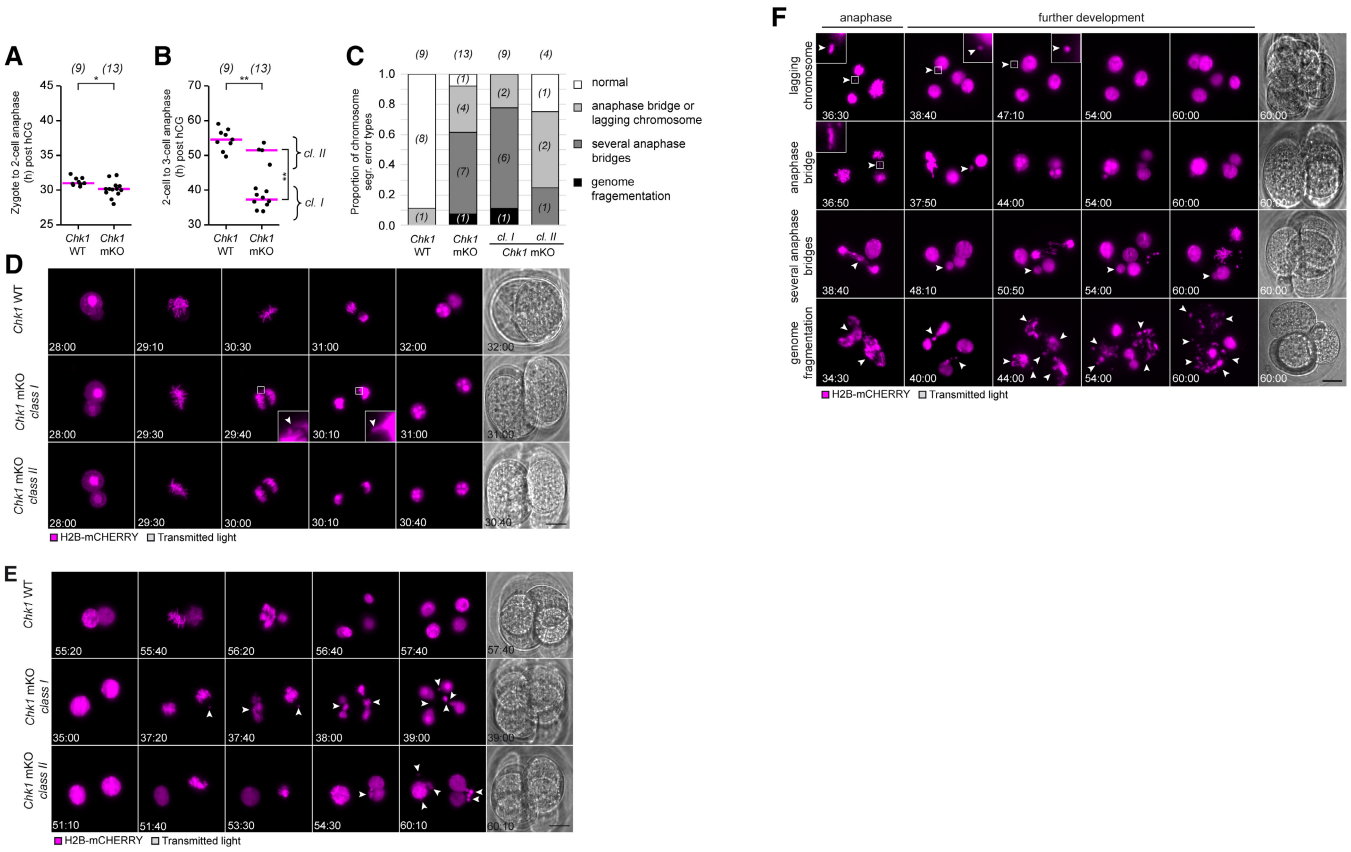

Figure EV4.

Figure EV4. CHK1 is essential for DNA integrity protection in the second embryonic division.

A, B Data from time-lapse light-sheet imaging (Fig 5B) were used to quantify initiation of anaphase (h) from zygote to two-cell (A) and time of division (h) from two-cell to three-cell (B) in *Chk1 WT* and *Chk1 mKO* embryos. A subgroup of *Chk1 mKO* embryos (*Chk1 mKO class I*) shows substantially accelerated second division. The median is shown. The data were pooled from two independent experiments. *$P = 0.01745$ (equal-variance *T*-test, two-sided). **$P < 0.01$ relative to *class I* (Kolmogorov–Smirnov test, two-sided), **$P < 0.01$ relative to *Chk1 WT* (Mann–Whitney *U*-test).

C Data from time-lapse light-sheet imaging (Fig 5B) were used to quantify the proportion of different types of chromosome segregation errors in embryos.

D–F Representative still images from time-lapse light-sheet imaging (Fig 5B) of the first embryonic division (D), second embryonic division (E), and different chromosome segregation error types (F) in wild-type (*Chk1 WT*), *Chk1 mKO class I*, and *Chk1 mKO class II* embryos. Embryos were microinjected, as shown in Fig 5A. Embryos expressing H2B-mCHERRY (magenta, chromosomes) are shown. Arrowheads mark different chromosome segregation error types. Scale bar 20 μm. See also related Movie EV6 (lagging chromosome, anaphase bridge, several anaphase bridges, and genome fragmentation).

Data information: The numbers in brackets denote the number of analyzed embryos per genotype.

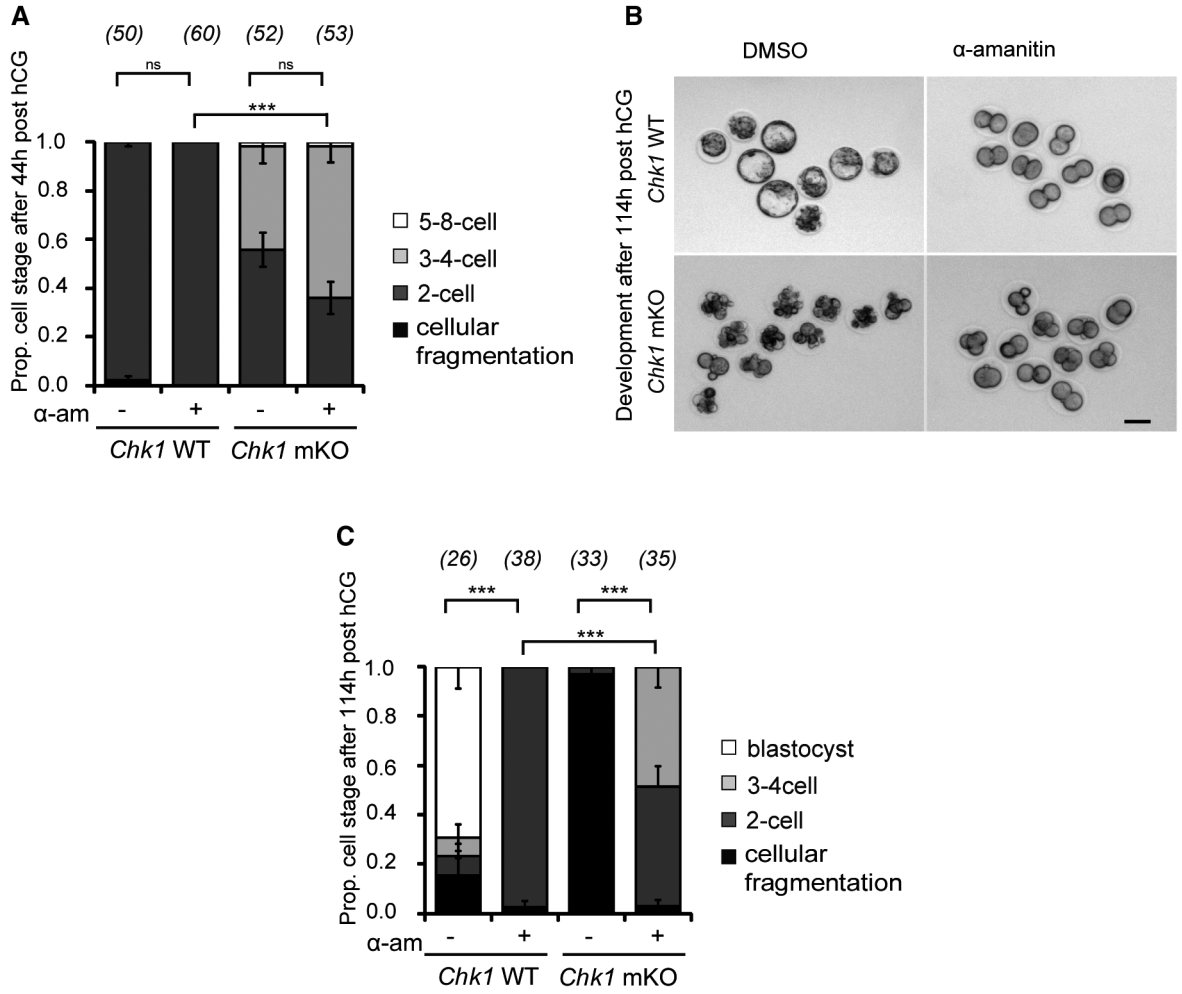

Figure EV5. CHK1 is necessary for the two-cell stage transcription block.

A Developmental analysis of *Chk1* WT and *Chk1* mKO embryos treated with α-amanitin (24 μg/ml) or DMSO. The embryos were scored at 44 h post-hCG administration. The numbers in parentheses denote the number of analyzed embryos per group. The data were pooled from two independent experiments. Strain background: CD-1 with small part C57J/BL6 and C57J/BL6 with small part CD-1. Error bars denote the standard error of the mean. ns, non-significant $P = 0.27113$ (*Chk1* WT), $P = 0.05605$ (*Chk1* mKO), ***$P = 0.00000$ (Cochran–Armitage trend test, two-sided).

B Representative images from developmental analysis (C) of developmental stages at 114 h post-hCG administration. Scale bar 60 μm.

C Developmental analysis of *Chk1 WT* and *Chk1 mKO* embryos treated with α-amanitin (24 μg/ml) or DMSO. The embryos were scored at 114 h post-hCG administration. The numbers in parentheses denote the number of analyzed embryos per group. The data were pooled from two independent experiments. Error bars denote the standard error of the mean. ***$P = 0.000$ (Cochran–Armitage trend test, two-sided).

Appendix File Table of Contents

Appendix Figure S1

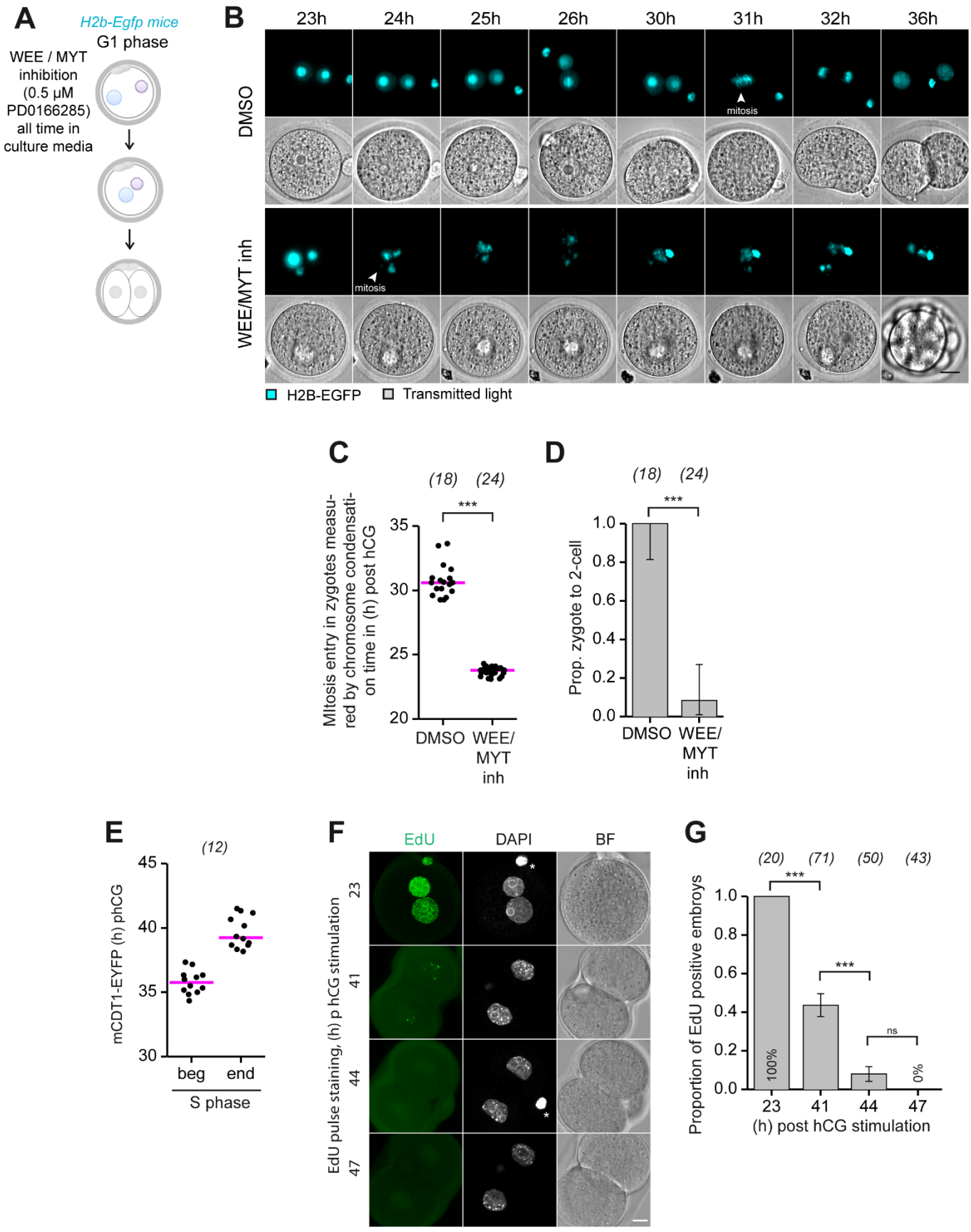

Appendix Figure S1 Characterisation of completing DNA replication and duration of S-phase

A Schematic of the experimental procedure.

B Representative still images from time-lapse light-sheet imaging of embryos from *H2b-Egfp* transgenic mice from 23 to 36 h post hCG administration after WEE/MYT kinase inhibition (as shown in **A**) or DMSO treatment (21 h post hCG administration). Embryos expressing H2B-EGFP (cyan, chromosomes) are shown. Transmitted light (grays). Arrows indicate mitotic entry. Scalebar 20 µm. See also related Movie EV1 (ctrl, WEE/MYT inhibition)

C Data from time-lapse light-sheet imaging (**B**) was used to quantify chromosome condensation time (h) from zygote to 2-cell stage embryos. The data were pooled from two independent experiments. Median is shown. ***p=0.00000 (Mann-Whitney U Test, two-sided).

D Data from time-lapse light-sheet imaging (**B**) was used to quantify the proportion of zygote to 2-cell development. The data were pooled from two independent experiments. Error bars denote the 95% confidence interval. ***p=0.0000 (Fisher's Exact Test, two-sided).

E Beginning and ending of S phase measured by mCDT1-EYFP sensor fluorescence signal in wild-type embryos using time-lapse light-sheet imaging. The magenta bar represents the median of the S phase beginning and ending.

F Representative images from analysis of S phase estimated by EdU pulse staining in wild-type embryos at 23, 41, 44, and 47 h post hCG administration. The embryos were fixed after a 60 min EdU pulse (green), and DNA was visualized by DAPI staining (grays, chromatin). BF (bright field). Asterisk mark polar bodies. Scalebar 10 µm.

G Data from immunofluorescence analysis (**F**) was used to quantify the proportion of EdU-positive embryos. Error bars denote the standard error of the mean. The data are from one experiment. ns non-significant p=0.1211, ***p=0.0000 (Fisher's Exact Test).

Appendix Figure S2

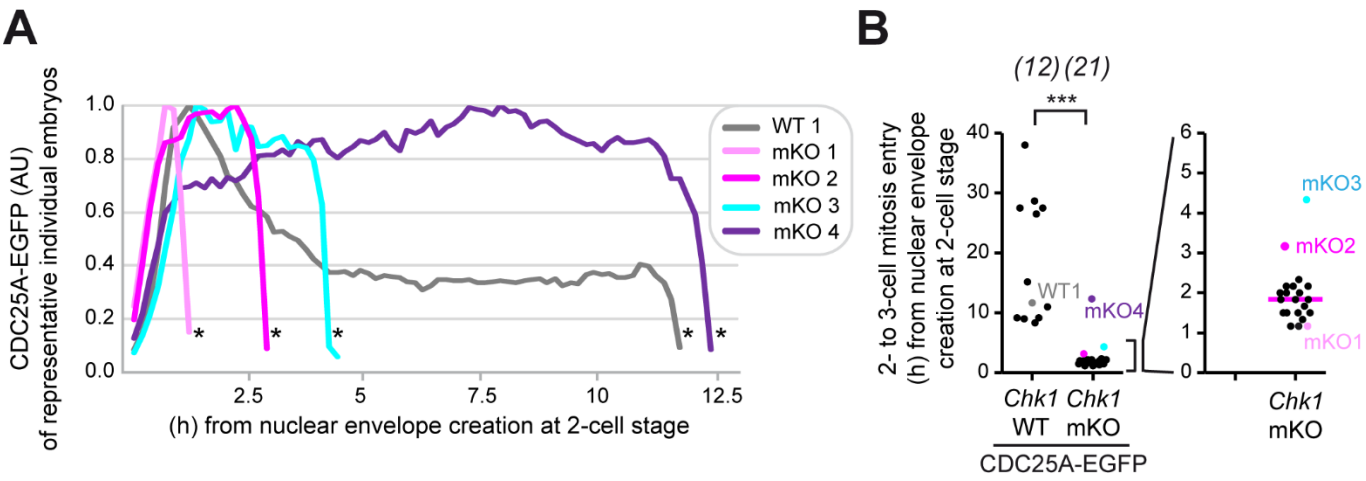

Appendix Figure S2 CHK1 kinase regulates long G2 in mouse 2-cell stage embryos by restraining CDK1 activity via CDC25A degradation

A Line chart of fluorescence signal intensity of CDC25A-EGFP of individual *Chk1 WT* and *Chk1 mKO* 2-cell stage embryos scanned using light-sheet time-lapse microscopy from nuclear envelope to 12,5 h after nuclear envelope formation. Embryos were microinjected as shown in **Fig 3B**. Asterisk mark signal drop after nuclear envelope breakdown (not degradation). The data are from one experiment with two *Chk1 WT* and four *Chk1 mKO* mice treated individually. The line of the *Chk1 WT* average is shown. The 2- to 3-cell anaphase timing is shown in Fig. EV3F.

B Data from time-lapse light-sheet imaging **(Fig 3B)** was used to quantify initiation of anaphase (h) from 2-cell to 3-cell in *Cdc25a*-microinjected *Chk1 WT*, and *Cdc25a*-microinjected *Chk1 mKO.* Median is shown. ***p=0.0000 (Mann-Whitney U test, two-sided).

Appendix Figure S3

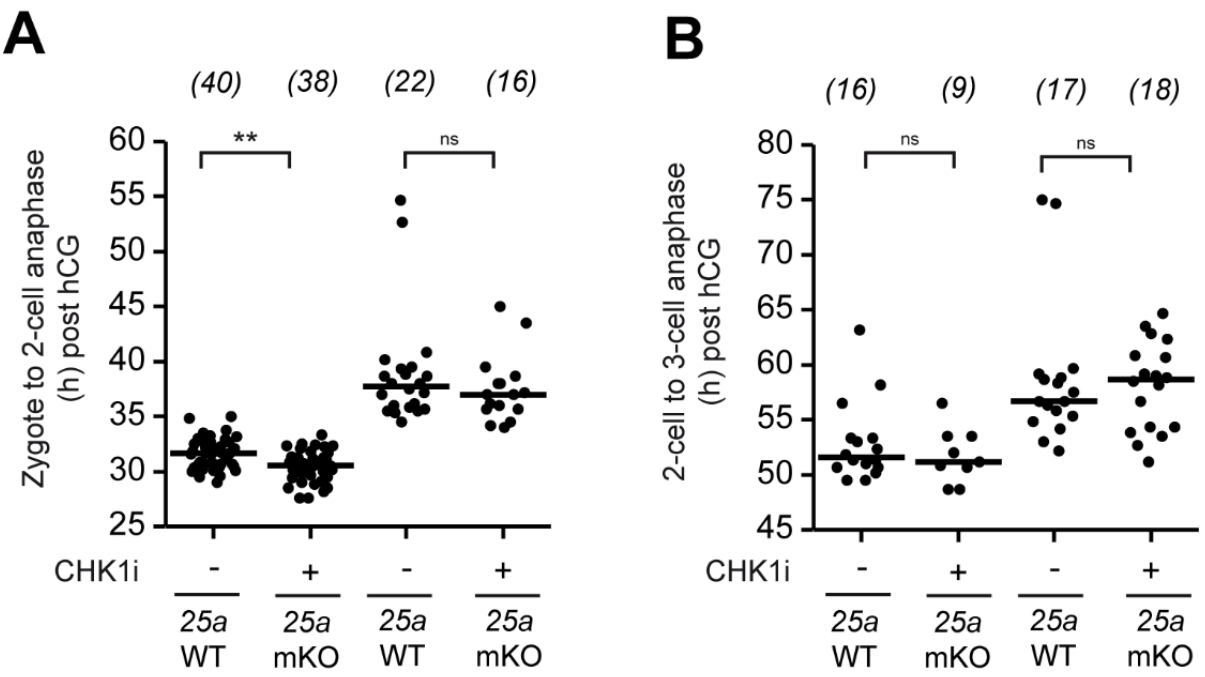

Appendix Figure S3 Effect of CHK1 inhibition on the timing of mitosis in *Cdc25a* mKO embryos.

A, B Dot-plot graph of division time (h) from zygote to 2-cell (**A**) and 2-cell to 3-cell stage (**B**) analyzed from time-lapse wide-field imaging of *Cdc25a* WT and *Cdc25a mKO* embryos. The embryos were treated with 250 nM CHIR-124. ns non-significant, **p<0.01 (Mann-Whitney U test, two-sided).